NEW MATHEMATICAL MODELS

OF

INERT GAS TRANSPORT THROUGH BIOLOGICAL

TISSUE IN HYPERBARIC ENVIRONMENTS

by

T.R. HENNESSY, M.Sc.

++++++++++++++++++++

A thesis submitted in fulfilment of the requirements for the Degree of Doctor in Philosophy in the University of Cape Town.

April, 1973

++++++++++++++++++++

STATEMENT

This is to certify that all ideas and results presented in this thesis are due to the writer, except where due reference is given.

No portion of this thesis has been previously submitted in support of an application for any other degree or qualification in this or any other University.

T.R. Hennessy.

April, 1973.

To explain all nature is too difficult a task for any one man or even for any one age.

It is much better to do a little with certainty and leave the rest for others that come after you than to explain all things without making sure of anything.

Isaac Newton.

1642-1727.

ABSTRACT

The thesis is concerned with a fundamental mathematical analysis of inert gas transport through biological tissue at a raised ambient partial pressure. Three basic time-scales of transport in tissue are defined and their relationship examined and compared with existing models, which are shown to be usually inadequate in one or more ways.

As a result three new mathematical models are proposed and solved both asymptotically and numerically. The first is applied to experimental data for non-perfused tissue which yields an improved value of the intracellular diffusion coefficient for nitrogen. An expression is also derived which should be useful in evaluating this constant and the volume fraction of extracellular fluid. The second embraces a number of current models and is applicable to perfused tissue. It should be useful in interpreting inert gas uptake curves The model is applied to experimental data, and a source of possible error is discovered in using experimental non-asymptotic time constants.

The third is a model which claims to resolve the controversy between the diffusion and perfusion theories of gas transport in tissue. The result is that in the large, diffusion is more important than perfusion, except in muscle tissue where they interact.

Three different methods of numerical inversion of the Laplace Transform are compared and one is shown to be the most useful for solving gas uptake problems.

The main result of the thesis is a contribution to the establishment of a mathematical basis for gas transport in various situations in the biological sphere.

TABLE of CONTENTS

CHAPTER ONE

INTRODUCTION

This study was at first undertaken from the main viewpoint of decompression theory. However it soon became clear as the work progressed that it would not be possible to discuss this topic which today has a vast literature. A crucial aspect of decompression theory revolves around the adequacy of a mathematical model of hyperbaric inert gas transport in the tissue type responsible for decompression sickness. Many different models have been proposed over the years from Haldane (1908) to Hills (1966). Thus there is adequate justification for the present study on these grounds alone.

With the advent of high altitude aviation there was a renewed interest in decompression theory from the hypobaric viewpoint. In addition, uptake and washout of radioactive inert gas tracers became popular as a means of measuring blood-flow and anaesthetic and other drug transport characteristics in various organs. In all these approaches, some sort of mathematical model is vitally necessary to describe the uptake or elimination rates of the various substances dissolved in the blood.

It was found that whilst one particular model seems to serve reasonably well in one situation, it would often fail in attempts to generalize it. This is mainly due to an inadequate establishment of the mathematical model and the approximations used to justify it.

In this thesis we propose three new models which have become necessary in the light of recent advances in the field of gas transport through tissue. In each case the assumptions

under which the model is valid are carefully detailed and an order of magnitude analysis reveals which quantities assume little importance in a given situation. Where possible the model is compared with available experimental data, and agreement is in all cases good.

Before introducing the contents of each chapter, we give a brief description of the general mode of uptake of an inert gas in tissue on exposure to an increased ambient pressure of that gas.

If the blood perfusion is operating normally, then the tissue zone is exposed at its arterial end to the full ambient pressure of the inert gas available directly from the inspired mixture. There is of course a drop in pressure due to water vapour dilution and transmission losses, but at a hyperbaric environment these are usually negligible. The applied inert gas pressure is supposed to be suddenly applied at zero time via a step-change in pressure from some initial state.

The artery now subdivides several times into smaller diameter vessels, finally reaching the capillary, normally 7 - 9μ in diameter. The inert gas may be assumed to have suffered very little transmission loss in this process, simply because of the thickness of the lining of the larger vessels. At the capillary level, the inert gas easily diffuses across the capillary membrane (which may be a barrier to other solutes or metabolites) and thence into the interstitial tissue, an aqueous fluid, which surrounds each

cell. The cells constitute over half the bulk of the tissue, and diffusion in this phase is the predominant factor.

This process continues until equilibrium is attained, which may occupy a few minutes to many hours, depending on the type of tissue and its blood perfusion.

From this we may define three different time scales describing the process:

(i) the perfusion time scale T_P , a measure of the time for a unit quantity of blood to serve a unit volume of tissue.

(ii) the interstitial time scale, T_I , a measure of the time for the gas to pass from the capillary to the vicinity of a cell.

(iii) the cellular time scale ,T_C , a measure of the time for the gas to diffuse into the cell.

These three quantities will be explained more fully in the relevant chapters, and a comparison is developed in chapter seven.

In living tissue there exists a wide spectrum of T_P . (See Table V) and also T_I . However it is believed that T_C is a constant, depending on the cell diameter, which is reasonably uniform. Many gas uptake experiments take place in excised tissue in the form of membranes and tissue slices. In this case T_I is large and perfusion is usually absent, thus $T_P = \infty$.

Now the circulation is designed around the efficient supply of oxygen to the cells and the removal of waste products (auto regulation). The perfusion time scale

(and interstitial time scale to a lesser extent) is a dynamic function of the metabolic state of the tissue, for example a low T_P for a high metabolic demand, and vice versa.

Thus it may be seen that a tissue zone either perfused or not may have a very wide spectrum of time scales T_P , T_I and T_C .

The mathematical model chosen to describe a particular situation depends heavily on the relationship that these three quantities have to each other.

Thus in chapter two a model of excised tissue is developed in which $T_P = \infty$ and it is shown that $T_I \sim T_C$. The analytical solution of the model is evaluated exactly at asymptotic times by a novel method, and numerically in chapter six.

A comparison with experimental data yields an improved value of the cellular diffusion time scale. This value is subsequently used in later chapters.

In chapter three, a model of perfused tissue is proposed in which $T_I \sim 0$, and $T_P \sim T_C$. It is shown that the model contains effectively nearly all other models of gas uptake in tissue, based upon a perfusion or diffusion approach.

A comparison with experiment highlights some inadequacies in present experimental approaches. A numerical solution of the model is given in chapter six.

Chapter four gives an equivalent diffusion analysis of a computer which has been proposed to describe gas transport

in tissue for predicting decompression formats. The time scale of the instrument is shown to agree closely in a non-linear manner with the cellular diffusion time scale of tissue, even though the computer was developed on a purely empirical basis (with regard to current models of gas uptake in tissue). This finding may be considered as a new mathematical model, based on the equivalent diffusion coefficient a linear function of the ambient pressure, but this possibility is discounted.

In chapter five we propose a model of gas uptake from the capillary. In the model we assume $T_I \sim 0$, and T_P , T_C arbitrary. The model includes axial dependence, a feature which has been either neglected or poorly treated in the past. It is shown that the current perfusion and diffusion theories are merely subcases of this model, and in chapter six, numerical solutions display this fact. Graphs are presented which show clearly where each theory is applicable, and the interaction zone is identified as being in muscle tissue.

The three time scales are discussed in chapter seven, and a comparison of various models is given, and linked to the results of the thesis.

Appendices A, B and C contain specialised mathematical and computational information used in the main body of the work.

CHAPTER TWO

A MODEL OF NON-PERFUSED TISSUE

2.1 Diffusion Coefficients in Excised Tissue

One of the earliest experiments in diffusion was that of the rate of flow of oxygen across a thin excised tissue slice. Krogh (1919) reports a value of $D \approx 1/3$ of that of oxygen in water ($\approx 10^{-5}$ cm^2 sec^{-1}). Similar results for nitrogen may also be extracted from this paper.

The normal method was to apply a fixed pressure gradient across the sample and measure the volume of nitrogen collected per unit time as soon as the steady state was reached. The rate of flow per unit area is simply proportional to the product of the pressure difference per unit thickness and the diffusion coefficient D by Fick's Law.

Thus $$\dot{V} = AD(P_1 - P_o)/\ell$$

where A is the cross-sectional area and ℓ the thickness of the sample and $\dot{V}$ the rate of volume flow from a partial pressure P_1 to a pressure P_o across the slice.

By varying the thickness of the slice given the applied partial pressure across the sample, he was able to deduce that biological tissue behaved as a simple homogeneous diffusion medium. The fact that the diffusion coefficient was smaller than that of water was easily explained by the fact that the microscopic structure was not a pure aqueous medium.

On a closer examination of this equation, it is seen that there is another possible explanation of the lower calculated diffusion coefficient. This is simply that the cells in the tissue form a greater barrier to the flow of nitrogen than

the mainly aqueous fluid surrounding them. If this is the case then it is clear that the effective cross-sectional area of the tissue slice permitting gas transport will be reduced by the proportion of obstructing cells. However, if this fact is unknown, then the value of D will be unwittingly reduced to account for the reduced volume flux of gas across the slice. It is thus possible that tissue may behave as a heterogeneous medium, notwithstanding Krogh's early results based on steady state experiments. For if the cells are only semi-permeable, then diffusing inert gas will tend to by-pass the cells in the steady state case, and no information will be gained about intracellular diffusion. In samples with a sparse cellular distribution, this may not be important. However in the majority of cases, cellular material occupies a considerable proportion of the tissue space, of the order of 50 - 60%.

Thus one is forced to employ experimental methods which are able to highlight cellular diffusion. Unfortunately it is not feasible at the present time to aggregate the cells close together without damaging their membranes, otherwise cellular diffusion measurements would be straightforward. Thus fully transient methods in various modes have been employed.

Hills (1966) gives a brief review of some transient models which attempt to distinguish between transport in extra and intracellular fluid.

Unfortunately a number of methods treat the cell membrane as a simple diffusion barrier, rather than the cell as a whole (membrane versus bulk diffusion). The former introduces

the so-called permeability coefficient (P) for mathematical convenience, since then the diffusion equation is reduced from a partial to an ordinary differential equation. From this, one can easily construct a bulk diffusion coefficient by multiplying the permeability coefficient by some characteristic diffusion path length, which we take to be the width of the cell. (L). Thus $D = P.L.$

Using this approximate technique the permeability data of Harris and Burn (1948) and that of Opatowski and Schmidt (1952) can be compared with bulk diffusion data of Dick (1958), Fenichel and Horowitz (1963) and Hills (1967). By taking L to be of the order of magnitude of a cell diameter (about 30μ), the overall value of the intra-cellular bulk diffusion coefficient of various substances appears to be about 10^{-10} cm^2 sec^{-1}. This value is about 10^{-4} times smaller than the diffusion coefficient in water.

Thus it is apparent that unless the diffusion experiment is transient (in the sense that the diffusing substance is forced to enter the cellular phase of the tissue), it will not be possible to notice the extremely small cellular uptake of the substance as it passes through a tissue sample. This will be shown mathematically at the end of the chapter.

At the present time, the very low values of the cellular diffusion coefficients seem to be viewed with caution in the literature. Thus it is remarkable that the cell can behave as an almost impermeable medium to various substances, whilst other biological membranes offer slight resistance. Another confusing aspect is the complexity of the mathematical model used to distinguish between extra and intra cellular diffusion.

Indeed 'the simpler the model, the more convincing the results' seems to be the approach adopted by physiologists. Obviously this is not necessarily true. Diffusion in heterogeneous tissue can be viewed as a complex process and any approximations must be carefully justified.

2.2 Diffusion into a rectangular tissue slice

It seems that skeletal rabbit muscle behaves as a heterogeneous diffusion medium in the uptake of inert non-polar gases (Hills, 1967). In demonstrating this phenomenon, a thin tissue slice is trimmed to the size of a microscope slide and inserted into a dilatometer. Acetylene gas is admitted to the evacuated chamber via a capillary tube and plugged with a pellet of mercury. Gas diffuses across the main cross-sectional area of the slice until it reaches the impermeable base and reflects back again. Some gas will also diffuse across the edges of the slice. During this process, gas will be forced to occupy the cellular space. The quantity of acetylene absorbed by the sample is then measured over a period of hours. Since this gas is about 70 times more soluble in aqueous fluids than nitrogen, the volume of gas absorbed is large, resulting in more accurate readings.

The curve of mass $M(t)$ versus time (t) is broken down into the sum of usually three well separated exponential components by backward projection.

If the tissue behaves as a homogeneous diffusion medium, then the solution of the linear gas diffusion equation predicts

k_{111} is about 6% greater than that obtained by neglecting edge effects.] However the other time constants k_{ijl} are all close together, with a_{ijl} not all small; backward projection simply cannot isolate these components which are important at small to medium times. This difficulty has been highlighted by van Liew (1962) who showed that an actual curve generated by eight close exponential components could also be closely fitted by one using only three more separated ones. Thus one must view with suspicion the usual interpretation of the largest time constant (important in the initial stages) extracted by backward projection from data curves where small effects may be expected to perturb gas uptake at initial stages. Future experiments must therefore eliminate side diffusion, if the uptake curve is to be analysed at small to medium times.

The only reliable time-constant that can be found is the smallest one k_1, which is extracted at the asymptotic stage of the experiment.

It can normally be measured accurately and, if the medium is homogeneous, provides the best means of determining the diffusion constant D.

If, however, there is no simple inverse square relationship between the asymptotic time-constants extracted, then this provides the strongest evidence of a heterogeneous diffusion medium. Accordingly it is necessary to propose a suitable mathematical model consisting of a fairly regular distribution of cells embedded in aqueous fluid. The main proof of the model is that it must at least predict the smallest time constant for different tissue dimensions and

ultimately the correct time course of gas uptake. It should be noted that it is not necessarily the diffusion constant D that may be non-linear, but rather the geometry of the tissue.

2.3 A New Mathematical Model of Heterogeneous Tissue.

A typical tissue slice is shown in Figure 1. Clearly gas diffuses rapidly through the extracellular region (diffusion constant D_e) and slowly into the cells (diffusion constant D_c). The cells are macroscopically well ordered and of uniform size and thus it is reasonable to assume that the area of cellular material allowing mass transfer with extracellular fluid is also uniform throughout the section. However, analysis of diffusion in the section is a formidable mathematical problem. The main feature of the gas uptake process in the section is one of interaction and feedback from the cells and impermeable base. Any mathematical model must be capable of highlighting this unusual effect, while at the same time not detracting from the normal diffusion in each phase.

It is important to realize that the effect of the impermeable base controls the particular form of the model chosen. If there are other boundary conditions, a quite different geometry may be necessary.

An interesting model has been effectively used by Hills (1967, 1968). However, linearization and approximation unfortunately obscure not only the asymptotic behaviour of his model, but also the role played by various vital dimensionless parameters, to be developed here.

Thus he chooses the slowest cellular growth component for studying the overall interaction. This is essentially a

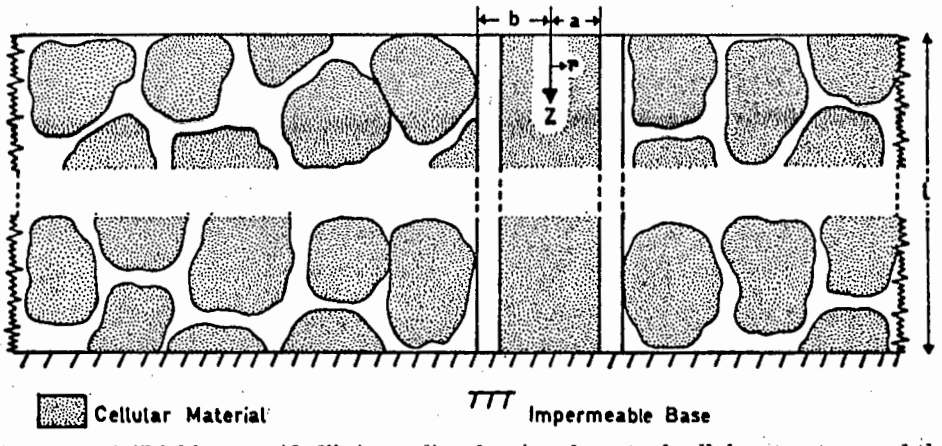

Figure 1. A "highly magnified" tissue slice showing the actual cellular structure and the proposed equivalent mathematical model of a typical cellular cylinder and extra cellular annulus

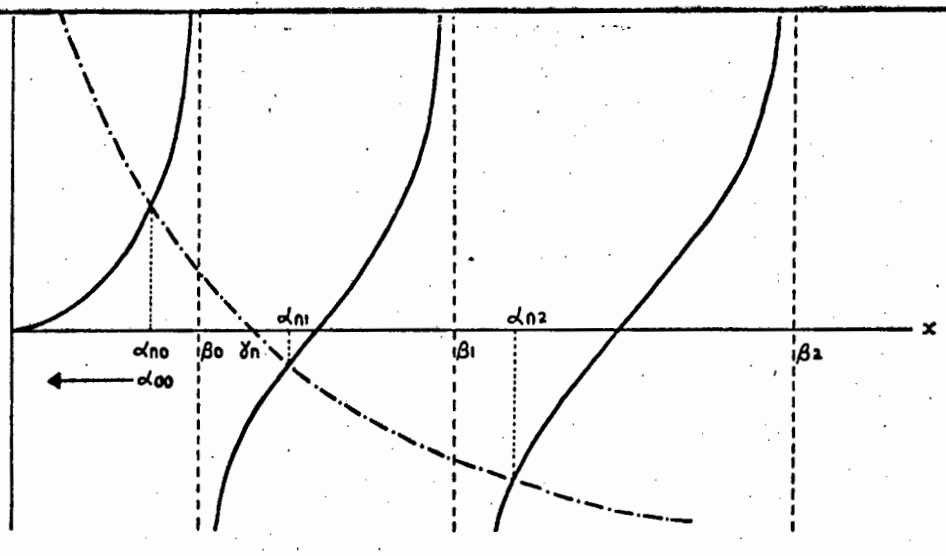

Figure 2. The curves $J_1(x)/J_0(x)$ (———) and $(\gamma_n^2 - x^2)/2\mu x$ (—·—·) (not to scale), showing that $\alpha_{n0} < \beta_{00}$ for all $n = 0, 1, \ldots$. The latter curve moves to the left with decreasing n and thus $\alpha_{00} < \beta_{00}$. Note that for $x < \gamma_n$ nearly all the roots $\alpha_{nl} \to \beta_l^-$, while for $x > \gamma_n$, $\alpha_{nl} \to \beta_{l-1}^+$. This effect is dominant for $\lambda \gg 1$ and thus γ_n.

purely asymptotic approach, since it implies that the extracellular space is nearly saturated. So faster time constants, for use at medium to small times, predicted by his analysis may not be valid at these said times, since the model is based upon the time being large. However the advantage is that his model actually avoids cells of a specific shape, but then a sacrifice of accuracy and linearization are inevitable.

In the present model, the cells are given a specific shape to reduce the problem to a tractable one, but the advantage gained will be that a careful error estimate of the magnitude of each term now becomes possible. In addition the model will be valid for all times.

Thus in the present configuration, a most reasonable simplification is to replace the cellular region by parallel cylinders of cellular material bounded by annuli of extracellular fluid, as shown in Figure 1.

Here one is assuming that the fraction of cross-sectional area of cellular material is effectively uniform in all planes parallel to the base. Any extracellular side-diffusion in between actual cells is easily accommodated by "thinning" down of the cellular cylinders. This model is fully capable of describing diffusion in both phases with mutual interaction and feedback.

Coordinates for a typical cylinder are chosen as shown in Figure 1. A pressure P_1 is applied to the face $z = 0$. The region is assumed to be at pressure P_o initially. The base of the cylinder is impermeable, as is the outer cylindrical surface, by symmetry.

Typical values of ℓ are 0.05 to 0.3 cm, whereas $b - a$ is of the order of cellular dimensions; viz., 15×10^{-4} cm. Thus radial diffusion time in the extracellular annulus may be ignored compared with axial diffusion.

Applying Fick's Law and mass balance to the annulus (pressure p_e), including side diffusion into the cellular cylinder, we have

$$\frac{\partial p_e}{\partial t} = D_e \frac{\partial^2 p_e}{\partial z^2} - \frac{2aD_c}{(b^2-a^2)} S_p \left(\frac{\partial p_c}{\partial r}\right)_{r=a} \qquad (2.3)$$

where $S_p = S_c/S_e$ is the partition coefficient of solubilities S_c and S_e in each region.

Also the usual diffusion equation is satisfied in the cellular cylinder (pressure p_c)

$$\frac{\partial p_c}{\partial t} = \frac{D_c}{r} \frac{\partial}{\partial r} \left(r \frac{\partial p_c}{\partial r}\right) + D_c \frac{\partial^2 p_c}{\partial z^2} \quad . \qquad (2.4)$$

The mass M of gas absorbed is given by mass flux across the face $z = 0$,

$$\frac{dM}{dt} = -\pi(b^2-a^2)S_e D_e \left(\frac{\partial p_e}{\partial z}\right)_{z=o} - \pi a^2 S_c D_c \left(\frac{\partial p_c}{\partial z}\right)_{z=o} \qquad (2.5)$$

Initial and boundary conditions are:

$$\begin{aligned} &\frac{\partial p_e}{\partial z} = \frac{\partial p_c}{\partial z} = 0 \ , \quad z = \ell, \quad t \geq 0 \ , \\ &p_e = p_c \ , \ r = a \ , \ t \geq 0 \ , \\ &p_e = p_c = P_o \ , \ t = 0 \ , \\ &p_e = p_c = P_1 \ , \ z = 0 \ , \ t > 0 \ . \end{aligned} \qquad (2.6)$$

Now we change to dimensionless variables defined by

$$t' = \frac{D_c t}{a^2} , \quad z' = z/\ell , \quad r' = r/a ,$$

$$P_e' = \frac{P_e - P_o}{P_1 - P_o} , \quad P_c' = \frac{P_c - P_o}{P_1 - P_o} , \quad M' = \frac{M - M_o}{M_\infty - M_o} , \tag{2.7}$$

where

$$M_\infty - M_o = \{\pi(b^2 - a^2)\ell S_e + \pi a^2 \ell S_c\}(P_1 - P_o) ,$$

M_o and M_∞ being the overall initial and final mass of inert gas in the tissue cylinder. Ignoring the primes, (2.3) reduces to

$$\frac{\partial p_e}{\partial t} = \lambda \frac{\partial^2 p_e}{\partial z^2} - 2\mu \left(\frac{\partial p_c}{\partial r}\right)_{r=1} , \tag{2.8}$$

where

$$\lambda = \frac{a^2/D_c}{\ell^2/D_e} = \frac{\text{Time Scale in cellular material}}{\text{Time Scale in extracellular material}} ,$$

$$\mu = \frac{S_p}{b^2/a^2 - 1} = \frac{a^2 S_c}{(b^2 - a^2)S_e} \tag{2.9}$$

$$= \frac{\text{Capacity of cellular material}}{\text{Capacity of extracellular material}}$$

It is expected that λ and $\mu \sim 1$, thereby emphasizing the mutual interaction of the two regions.

Equation (2.4) reduces to

$$\frac{\partial p_c}{\partial t} = \frac{1}{r} \frac{\partial}{\partial r} \left(r \frac{\partial p_c}{\partial r}\right) , \tag{2.10}$$

where the term $a^2/\ell^2(\partial^2 p_c/\partial z^2)$ has been ignored since $a^2/\ell^2 \sim 25 \times 10^{-6}$.

Now as we have seen, it is expected that $D_c/D_e \sim 10^{-4}$ and thus the second term on the right-hand side of (2.5) can be ignored.

Thus (2.5) simplies to

$$\frac{dM}{dt} = -\frac{\lambda}{1+\mu}\left(\frac{\partial p_e}{\partial z}\right)_{z=o} . \tag{2.11}$$

The boundary and initial conditions may be restated as:

$$\begin{aligned} &\frac{\partial p_e}{\partial z} = \frac{\partial p_c}{\partial z} = 0 , \quad z = 1 , \ t \geq 0 , \\ &p_e = p_c = 0 , \quad t = 0 , \\ &p_e = p_c , \ r = 1 , \ t \geq 0 , \\ &p_e = 1 , \ z = 0 , \ t > 0 . \end{aligned} \tag{2.12}$$

Note that the boundary condition $p_c = 1$, $z = 0$ has been removed, otherwise the equations become over-determined. The reason for this is that, by imposing this condition, an axial cellular diffusion gradient over and above that generated by side diffusion from the extracellular region is implied, and yet such small gradient has been ignored in (2.10).

However, this adjustment fortunately turns out to be negligible in evaluating the mass uptake, on the same ground as that used in establishing (2.11).

The Laplace Transform $\bar{F}(s) = \int_o^\infty e^{-st} F(t)dt$ is applied to (2.8), (2.10), (2.11) and (2.12), yielding a set of ordinary differential equations where the time variable has been removed (Churchill, 1958).

Solution is straightforward with the results

$$\begin{aligned} \bar{p}_e &= \frac{1}{s}\,\frac{\cosh \sqrt{\theta}(1-z)}{\cosh \sqrt{\theta}} , \\ \bar{p}_c &= \frac{1}{s}\,\frac{\cosh \sqrt{\theta}(1-z)\ I_o(\sqrt{s}r)}{\cosh \sqrt{\theta}\quad I_o(\sqrt{s})} , \end{aligned} \tag{2.13}$$

with

$$\lambda\theta = s + 2\mu\sqrt{s}\,\frac{I_1(\sqrt{s})}{I_o(\sqrt{s})} \quad , \tag{2.14}$$

and

$$\bar{M}(s) = \frac{\lambda}{1+\mu}\,\frac{\sqrt{\theta}}{s^2}\,\tanh\sqrt{\theta} \quad . \tag{2.15}$$

The symbols I_o and I_1 denote the modified Bessel functions of order zero and one. Their properties are fully described in Abramovitz and Stegun (1965).

We are primarily interested in the inversion of (2.15), especially at large times, that is for small values of s.

It can be seen that $\bar{M}(s)$ has singularities at the points s given by

(i) $s = 0$,

(ii) $s = -\beta_m^2$ where $J_o(\beta_m) = 0$, $m = 0,1,2, \ldots$, (2.16)

(iii) $s + 2\mu\sqrt{s}\,\frac{I_1(\sqrt{s})}{I_o(\sqrt{s})} = -(2n+1)^2\pi^2\lambda/4 = -\gamma_n^2$, $n = 0,1,2,\ldots$

Note that $I_o(ix) = J_o(x)$, $I_1(ix) = iJ_1(x)$.

The residue at $s = 0$ is easily evaluated and is unity, as to be expected since $M(t) \to 1$ as $t \to \infty$.

By attempting to form the Laurent expansion of $\bar{M}(s)$ at the points $s = -\beta_m^2$, it can be shown that these points are isolated essential singularities and the residue cannot easily be evaluated beyond a few terms in the series. It is found that the residues here represent in the large, diffusion into the solid cellular cylinder plus the effect of multiple feed back from the cellular region. This is evidenced by the fact that the singularities are governed by the roots of $J_o(x) = 0$, as in normal straight diffusion into a solid cylinder (Crank, 1956).

It is not too difficult to show that the roots of (2.16) (iii) are all simple poles, and further that they are all real and negative. [See Appendix C] .

If we put $s = -\alpha_n^2$, then α_n is a positive root of

$$\alpha_n^2 + 2\mu\alpha_n \frac{J_1(\alpha_n)}{J_o(\alpha_n)} = \gamma_n^2 \quad . \tag{2.17}$$

Note that for each $n = 0,1,2, \ldots$ there are an infinity of roots, thus implying a double infinite series for the residue at these points. Since the poles are simple, the residue is

$$\frac{\lambda}{1+\mu} \frac{e^{st}}{s^2} \frac{\sqrt{\theta}\sinh\sqrt{\theta}}{\frac{d}{ds}(\cosh\sqrt{\theta})}\Bigg|_{s=-\alpha_n^2} \quad .$$

After some reduction, the result is

$$-\frac{2\lambda\gamma_n^2 e^{-\alpha_n^2 t}}{(1+\mu)\alpha_n^4(1+\mu+\mu J_1^2(\alpha_n)/J_o^2(\alpha_n))} \quad .$$

Thus summing the residues at all the singularities, we have

$$M(t) = 1 - \frac{2\lambda}{1+\mu} \sum_{n=o}^{\infty} \sum_{i=o}^{\infty} a_{ni} e^{-\alpha_{ni}^2 t} + \sum_{m=o}^{\infty} R_m(t,\beta_m). \tag{2.18}$$

where $R_m(t,\beta_m)$ is the residue at the isolated essential singularity $s = -\beta_m^2$, and

$$a_{nt} = \gamma_n^2/\alpha_{ni}^4(1 + \mu + \mu J_1^2/J_o^2), \tag{2.19}$$

where α_{ni} are the roots of (2.17) for each n .

To determine the asymptotic behaviour of $M(t)$, the nearest singularity to the origin must be found. The residue at this point will control the asymptotic form of $M(t)$ before $s = 0$ or $t = \infty$ is reached. Now the nearest singularity will

be either at $s = -\alpha_{oo}^2$ or $s = -\beta_o^2$ depending on which is smaller. Each separately is the smallest root of (2.16)(ii) and (iii).

In Figure 2, $J_1(x)/J_o(x)$ is plotted against $(\gamma_n^2-x^2)/2\mu x$. Clearly the smallest root is α_{oo} and is less than β_o which is the smallest root of $J_o(x) = 0$. Thus α_{oo} controls the asymptotic behaviour of $M(t)$, and it is thus unnecessary to evaluate any of the terms R_m for this purpose.

Hence

$$M(t) \sim 1 - A\, e^{-\alpha^2 t} \quad , \tag{2.20}$$

where α is the smallest root of

$$\alpha^2 + 2\mu\alpha \frac{J_1(\alpha)}{J_o(\alpha)} = \pi^2\lambda/4 \quad , \tag{2.21}$$

and

$$A = \frac{\pi^2\lambda^2}{2(1+\mu)} / \alpha^4[1 + \mu + \mu J_1^2(\alpha)J_o^2(\alpha)] \quad . \tag{2.21'}$$

If $M(t)$ and t are now measured in dimensional units, (2.20) may be converted with $D_c t/b^2$ replacing t in (2.20).

Note that, if $\mu = 0$, then $M(t)$ reduces to the standard solution of diffusion into a homogeneous slab, since the singularities at $s = -\beta_m^2$ disappear and $\alpha_n^2 = (2n+1)^2\pi^2\lambda/4$ as to be expected.

If $\lambda >> 1$, implying slow diffusion into the cellular region, or fast diffusion into the extra-cellular region, then the first series in (2.18) decays rapidly in time, since nearly all the roots α_{ni} approach the roots of $J_o(x) = 0$, which means that the a_{ni} tend to zero; the remaining roots are large. (See Fig. 2.)

The second series thus represents mostly diffusion into a

solid cellular cylinder and in this case dominates the asymptotic behaviour of M(t). However this form is still given by (2.20), since $\alpha_{oo} \sim \beta_o$, but here A will be rather derived from the solution of diffusion straight into the cellular cylinder, since the extracellular region will be equilibrated very rapidly. In other words (2.21) may always be used with confidence whatever the value of λ. Only A may be an unreliable parameter.

Clearly the double series in (2.18) represents in the large diffusion into the extracellular region plus interaction with initially the so-called "fast" components of the cellular region, as the gas diffuses down to the impermeable base and reflects back. Subsequent interaction is between the slower components. The phenomenon of mutual interaction (multiple feed-back)between cellular and extracellular fluid is thus fully present in the model.

The interesting point is that it is the first series which controls the asymptotic behaviour of M(t), if λ is not large. The reason is that if λ is of order one, then the time scales in each region are similar, and the asymototic behaviour will be one of interaction between the slowest components of each system, as controlled by the first series. This is actually the basis of Hills (1968) assumption that the overall response is effectively governed by the two slowest exponential components of the cellular region. Clearly this approach is only valid for $\lambda > 1$, which fortunately turns out to be the oase, in the range of values used in his experiments.

If on the other hand $\lambda << 1$, implying fast cellular

diffusion compared with slow extracellular diffusion, typically in a tissue slice where $\ell \gg 0.3$ cm, then simple linear diffusion into a slab is the dominating feature and the asymptotic time constant from (2.21) closely approaches $(\pi^2/4)\lambda$, as is to be expected.

Thus it appears that (2.21) may be used whatever the tissue thickness ℓ, providing $D_c \ll D_e$. Naturally the effect of cellular diffusion is best demonstrated in cases where ℓ is very small. A tissue slice is however difficult to prepare in this case, and the present analysis is the only alternative.

If it is suspected that D_c is <u>not</u> very much less than D_e, then the approximations used in establishing (2.10) and (2.11) then become invalid, and a numerical solution of the full partial differential equation would be necessary.

2.4 Small-time Solution

It is of interest to obtain the small time solution of (2.15) and to compare it with the equivalent solution of linear diffusion into a homogeneous slab.

As $t \to 0$, $s \to \infty$, and to a first approximation (Abramovitz and Stegun, 1965),

$$\frac{I_1(s)}{I_0(s)} \sim 1 - 1/2s$$

thus $$\lambda\theta \sim s + 2\mu\sqrt{s} - \mu,$$

and $$\tanh\sqrt{\theta} \sim 1,$$

thus $$\bar{M}(s) \sim \frac{\sqrt{\lambda}}{1+\mu} \frac{(s + 2\mu\sqrt{s} - \mu)^{\frac{1}{2}}}{s^2}.$$

Note that apart from the double pole $s = 0$, the singularities of this function are now branch points, instead of simple poles as in (2.16)(iii).

Inversion of this function is preferably evaluated as a power series for purposes of comparison.

In any case, the closed form inversion does not appear in Roberts and Kaufman (1966) exhaustive table of Laplace Transforms, and we have already made an approximation to the first order.

Thus expanding for large s, we have

$$\bar{M}(s) \sim \frac{\sqrt{\lambda}}{1+\mu} \left({}^{1}/_{s}{}^{3/2} + \mu/s^{2} - \mu(1+\mu)/2s^{5/2} \ldots . \right)$$

valid, to a first order approximation of I_1/I_o.

Inversion is now completed term by term.

The result is

$$M(t) \sim \frac{\sqrt{\lambda}}{1+\mu} \left(2\sqrt{\frac{t}{\pi}} + \mu t - \frac{2}{3}\mu(1+\mu) \frac{t^{3/2}}{\sqrt{\pi}} \right) \qquad (2.22)$$

For the homogeneous case, $\mu = 0$ and thus

$$M_h(t) \simeq 2 \sqrt{\lambda t}/_{\pi}$$

This is to be compared with the expression given by (2.22) which represents the actual mass uptake. It is easily seen that the proportionate difference to a first approximation is $\mu M(t)$. In practice it is doubtful if this difference would be noticed, especially since it is very difficult to obtain accurate experimental data at small times. This again serves to demonstrate that it is very simple to mistakenly interpret gas uptake data in terms of a homogeneous model, by adjusting parameters. (In this case λ or μ would be increased or decreased accordingly so that $M_h(t)$ would agree with the observed values, represented exactly by $M(t)$.

2.5 Experimental Determination of the Parameters.

The asymptotic time-constant $k(= \alpha^2 D_c/a^2 \ min^{-1})$ is usually measured accurately by backward projection. Writing $x = b/\sqrt{D_c}$, an unknown, and substituting into (2.21), we have

$$2\mu \frac{\sqrt{k}}{x} \frac{J_1(\sqrt{k}x)}{J_o(\sqrt{k}x)} = \pi^2 D_e/4\ell^2 - k \ . \qquad (2.23)$$

This equation contains the unknowns x , μ and D_e , although the latter constant may easily be obtained in a separate steady state experiment, where the impermeable base is removed. It is normally difficult to measure A accurately, and thus (2.21') may prove unreliable. It is much simpler to perform several experiments with different tissue thickness values of ℓ . From the resulting set of equations (2.23), μ and x may be determined from a computer program. Since it is expected that $2a$ is a typical cell diameter usually 30×10^{-4} cm, D_c follows immediately. If further the partition coefficient S_p is known, then the volume fraction f of extracellular fluid follows from

$$f = \frac{S_p}{S_p + \mu} \ .$$

Best fit numerical values were evaluated with the aid of (2.23), using asymptotic time constants determined by Hills (1967) in the case of acetylene. The thinnest tissue-sample data were selected on the basis that λ should be as large as possible for (2.23) to be most effective.

Also the effects of edge diffusion

TABLE I

Comparison of Cellular Diffusion Time Scales for Nitrogen

Mathematical Model	Source	$D_c/a^2 min^{-1}$
Linear diffusion	Hempleman (1969)	0.00321
Non-linear gas resistor	Weaver (1968)	0.00376*
Cylindrical interaction	This Analysis	0.00423
Radial diffusion	Hills (1969)	0.00516†
Linear interaction	Hills (1967)	0.00538#

* Equivalent diffusion constant a linear function of pressure: mean value 0.00247, max. value 0.00376 in the range 0 to 100 p.s.i.a. (Hennessy, 1973). See Chapter 4 for details.

† Mean value.

Based on acetylene data, with Graham's Law correction.

and the release of other gases from the sample should be minimal in these cases.

The results were $\mu = 1.11$ and $D_c/a^2 = 0.00439\ min^{-1}$ as compared with Hills' value $0.00579\ min^{-1}$.

If further $S_p \sim 1$, the percentage of extracellular fluid is about 47%, comparable to the 38% for the average human (Guyton, 1969).

In Table I, a comparison of the parameter D_c/a^2 extracted from various sources is shown. All values are close together, providing ample evidence of the importance of diffusion in gas uptake in tissue.

2.6 Cellular Diffusion Coefficients

If we take a to be 15×10^{-4} cm , D_c of nitrogen takes on a value of about $1.6 \times 10^{-10} cm^2 \, sec^{-1}$. This is about 10^5 smaller than the diffusion coefficient in water.

Fenichel and Horowitz (1963) point out that this value is close to the self-diffusion coefficient of ice. They suggest that cytoplasmic (intracellular) water represents an orderly lattice which has properties of presenting a great diffusion barrier to a wide variety of substances.

Recently Hills (1970) has presented an analysis which shows that even oxygen as a metabolic gas may have a similar very low intracellular diffusion coefficient. His model determines a lower bound to the cellular diffusion coefficient for oxygen, in order that no cell or its centre can ever become anoxic in a normal metabolic state.

Thus it seems clear that any model of gas transport in biological tissue at hyperbaric exposure must take into account intracellular diffusion; with its own characteristic diffusion time scale.

In the case of tissue with perfusion, another time scale is introduced, in addition to the cellular and extracellular time scales. Here it is usual to assume that in this case, the extracellular region becomes "fully stirred" by hydrodynamic action. In the next chapter it will be shown that this situation is capable of an exact solution which is identical in form to the asymptotic solution of this chapter. The implication here is that the asymptotic solution of the present model could just as easily be obtained by assuming that the extracellular fluid was "fully stirred" at large times.

However, this assumption would lead to a very poor approximation to the solution at small to medium times, where the role played by extracellular diffusion would be completely masked. As has been pointed out earlier, Hills (1967, 1968) uses this technique to produce three dominant time constants, and it is doubtful if these constants accurately describe the gas uptake behaviour at non-asymptotic times in the thickest tissue samples. In any event the "fully stirred" approximation is only applicable in the case $\lambda >> 1$ where extracellular diffusion is much faster than that in the cellular region.

It should be pointed out that the technique of backward projection forces the gas uptake curve into the sum of three well defined exponential components. However the interpretation of these components is heavily dependent upon the mathematical model chosen and the relative magnitude of its parameters. In other words it is conceivable that a given mass uptake curve may be closely simulated by two fairly different mathematical models, each with different parameters, one which predicts an exponential series of close-time constants, the other series of well-separated constants. Thus one model may be as good as another over a wide range of physical applications. Also it is known that simple linear and cylindrical mass uptake closely approximate each other in time, providing dimensionless parameters are adjusted slightly (Crank, 1956). Thus instead of the present cylindrical model linear sheets of cellular material could have replaced the cells. However the analysis is no simpler and indeed it was found that the parameters D_c/b^2 and μ had to be adjusted by rather unrealistic factors to fit the data.

2.7 Steady State Diffusion

The most popular method of determining the diffusion constant in a homogeneous slab is by measuring the steady state mass flux from one face, the other being kept at some fixed partial pressure. In the case of heterogeneous tissue, the gas will by-pass the cellular region at the steady state stage. This method will thus give a means of measuring D_e and μ. Before the steady state is reached, however, there will be some interaction between the two regions and it seems worthwhile to at least obtain the asymptotic solution. We remove the boundary conditions $\partial p_e/\partial z = \partial p_c/\partial z = 0$ at $z = \ell$ in (2.12) and replace it by $p_e = p_c = 0$ at $z = \ell$.

The Laplace Transform solution is

$$\overline{p_e} = \frac{1}{s} \frac{\sinh \sqrt{\theta}(1-z)}{\sinh \sqrt{\theta}} \tag{2.24}$$

where θ is defined by (2.14).

Mass flux from the face $z = 0$ is given by

$$\frac{dM}{dt} = - \frac{\lambda}{1+\mu} \left(\frac{\partial p_e}{\partial z}\right)_{z=1} , \tag{2.25}$$

where the contribution from the cellular cross-sectional area is again ignored if $D_c << D_e$. Thus

$$\bar{M} = \frac{\lambda}{1+\mu} \frac{1}{s^2} \frac{\sqrt{\theta}}{\sinh \sqrt{\theta}} .$$

The singularities of $\bar{M}(s)$ are as in (2.16) except that here $\gamma_n^2 = n^2\pi^2\lambda$, $n = 0,1,2 \ldots$ The residue at the double pole $s = 0$ is easily evaluated by the Laurent series technique and is $\lambda t/(1 + \mu) - \frac{1}{6}$. The nearest singularity to the origin $s = 0$ is $s = - \alpha^2$, with $n = 1$ where

$$\alpha^2 + 2\mu\alpha \frac{J_1(\alpha)}{J_o(\alpha)} = \pi^2\lambda , \tag{2.26}$$

and hence

$$M(t) \sim \frac{\lambda t}{1+\mu} - \frac{1}{6} - A' e^{-\alpha^2 t} \quad . \qquad (2.27)$$

The value of A' can be found in the same way as for A .

If $\mu = 0$, (2.27) reduces to the exact solution for a homogeneous slab.

The time constant $k(= \alpha^2 D_c/a^2 \ min^{-1})$ can be determined by backward projection and D_c/a^2 and ℓ computed from (2.26) over several runs with different thickness values of ℓ.

Now it should be noted that α is likely to be large if λ is large since $\pi^2 \sim 10$ [see (2.26)] , and thus it may be difficult to evaluate accurately. This means that the larger the time scale in the cellular region, the more difficult it becomes to determine D_c by this method. In fact it would just be assumed that the tissue behaves as a homogeneous fast diffusion medium. Only if μ is large would there appear to be any discrepancy in the experimental results, and in any case the value of D_e would simply be "adjusted" to suit the homogeneous theory.

This can be seen by examining the steady state mass flux (using dimensional units).

We have in the heterogenous case

$$\dot{M} = D_e/(1+\mu)\ell^2 \quad \text{per unit area,}$$

and in the homogeneous case ($\mu = 0$)

$$\dot{M}_h = (D_e)_h/\ell^2 \quad \text{per unit area.}$$

Hence given a set of experimental data for $\dot{M}$, it is seen that the homogeneous diffusion coefficient is given by

$$(D_e)_h = \frac{D_e}{1+\mu} \simeq \frac{1}{2} D_e$$

which is in good agreement with the observed drop in values for the diffusion coefficient in water (Krogh 1919).

CHAPTER THREE

A MODEL OF PERFUSED TISSUE

3.1 Introduction

In the previous chapter a mathematical model was proposed to account for the observed interaction between the cellular and extracellular phases of an excised tissue sample when exposed to an inert gas. It was shown that if the ratio of the diffusion time scales in each phase is of order unity, then such interaction is rate contributing to the overall asymptotic uptake of the gas.

In living tissue, it is suggested that there are three time scales to be considered when an organ is exposed to a hyperbaric inert gas. There is the (i) perfusion time scale, the reciprocal of the volume of blood serving a unit volume of tissue per minute ($\dot{Q}$), (ii) the extracellular diffusion time scale, generally assumed to be very small, and (iii) the intracellular diffusion time scale, which as we have seen in chapter two may be very large.

In this chapter, therefore, it is proposed to examine the case of the blood/lymph perfusion time scale interacting with that of the cellular phase. Thus a tractable mathematical model is proposed to describe transient inert gas diffusion in heterogeneous tissue with perfusion controlling gas input to the cellular region. The corresponding solution of overall mass uptake of the inert gas is derived exactly and should be useful in interpreting washout curves from particular tissue zones, whether there is any interaction with cellular diffusion or not. It is shown that the solution contains effectively

nearly all models hitherto proposed to describe gas uptake in tissue.

Thus defining λ here to be the ratio $(a^2/D_c)/(1/\dot{Q}_e)$, where $\dot{Q}_e$ is the extracellular perfusion; D_c, the cellular diffusion coefficient; and $2a$, a typical cell diameter, it will be supposed that $\lambda \sim 1$.

The case of $\lambda << 1$ (that is perfusion more important than diffusion) has been discussed in the literature and forms the basis of the so-called "perfusion theory" in applications to decompression sickness and washout of inert tracers from living tissue. Undoubtedly there are "fast" zones where $\lambda << 1$.

The case of $\lambda >> 1$ (that is diffusion more important than perfusion) forms the basis of the so-called "diffusion theory" in decompression (Hempleman, 1969; Hills, 1969) and once again there are "slow" zones where $\lambda >> 1$.

A preliminary analysis of the case $\lambda \sim 1$ has also been undertaken by Hills (1967) in analysing the time-constants of washout of ^{85}Krypton from rabbit muscle. However his analysis of the mass balance equation in the equilibrated extracellular phase omits the loss of gas by diffusion into the cellular phase. In cases of $\lambda \sim 1$, this omission may be non-negligible. Also any linearization can be avoided as an exact solution of the time-constants can be obtained, if one accepts the present model.

3.2 The Mathematical Model

It is generally accepted that the extracellular region

behaves as though fully stirred, that is there are effectively no diffusion gradients in this region. Reasons for this assumption are that the diffusion time scale in the essentially aqueous extracellular phase is very small, in competition with typical perfusion time scales, especially as there appears to be some intercapillary perfusion in the form of lymph drainage.

However it is important to realize that there may well be tissue zones where the latter effect is negligible and coupled with larger intercapillary distances the interstitial diffusion time scale can no longer be ignored at small to medium times in comparison with that of blood perfusion and cellular diffusion.

In this case the assumption of full stirring would at best be only an asymptotic approximation to the interaction between blood perfusion and interstitial diffusion. Subsequent analysis by backward projection of an experimental washout curve in such a zone will be misleading in the interpretation of the earlier time constants extracted. Careful examination of the histology of such zones will be needed to set up a mathematical model valid for small to medium times.

However here we proceed with the assumption that the extracellular region is fully stirred.

Now the actual interstitial perfusion is unknown. However if it is assumed that the solubility partition coefficient between blood and interstitial fluid is of order unity, as is usually the case, then one may define an effective perfusion $\mathring{Q}$ (ml/ml tissue/minute) to the tissue consisting of the sum of actual blood and interstitial perfusion.

Also $\dot{Q} = \dot{Q}_e/f$, where f is the volume fraction of extracellular fluid.

The "fully stirred" assumption implies that the inert gas partial pressure p_e in the extracellular region is equal to the output venous pressure. Input arterial pressure is taken to be p_a .

Before proceeding further, a tractable mathematical model of the cellular space must be chosen. The cells are known to be macroscopically regular and well-spaced, and it may thus be assumed that each cell has a uniform surface area available for gas transfer from the extracellular region and a uniform volume, per unit volume of tissue. However it is also known that there is some contact between individual cells. Clearly, assuming a linear rectangular cellular space is too drastic, while a spherical space too optimistic. In the circumstances a cylindrical cellular space seems reasonable since it can allow for contact between a few cells by modifying the length of the average cylinder.

Further grounds for its adoption are that diffusion into living tissue is essentially a radial phenomenon, especially into skeletal muscle fibres, and that a cylinder has a shape factor of 2, as defined by Hills (1967). This factor is the closest mean value of a tractable model ranging from a rectangular to a spherical space.

However it should be noted that the choice of a cylindrical cellular space does not necessarily imply that the cells are actually cylindrical themselves. The particular geometric shape chosen merely aids the mathematics, and preselects

the most suitable diffusion surface area to volume ratio, while closely approximating histological macroscopic structure.

Accordingly, we define the radius and length of a typical cell by a and ℓ, respectively, and the radius of the extracellular annulus about the cell by b. The volume fraction of extracellular fluid f is thus given by

$$f = 1 - a^2/b^2 , \tag{3.1}$$

and μ, the ratio of inert gas capacity of cellular to extracellular fluid satisfies

$$\mu = \frac{S_p}{b^2/a^2 - 1} , \tag{3.2}$$

where S_p is the partition coefficient of cellular solubility S_c and extracellular S_e.

Consider the mass balance in the extracellular annulus. The equation takes the form of net mass influx by perfusion less mass flux into the cell equals mass build up in the extracellular annulus. Thus after some reduction, this equation may be written as

$$\frac{\partial p_e}{\partial t} = \frac{\dot{Q}}{f} (p_a - p_e) - 2\mu \frac{D_c}{a} \left(\frac{\partial p_c}{\partial r}\right)_{r=a} , \tag{3.3}$$

where p_c is the inert gas partial pressure in the cell. Notice that it has been assumed that both blood and interstitial fluid <u>input</u> pressures have a common value, p_a, later leaving the tissue at equilibrium pressure p_e.

Equation (3.3) has an exact analogue in heat conduction from a fully stirred fluid into a cylinder, with radiation heat loss to the surroundings and possibly a constant input of heat to the stirred volume (cf. Carslaw & Jaeger, 1959, page 329).

The diffusion equation is satisfied in the cell:

$$\frac{\partial p_c}{\partial t} = \frac{D_c}{r}\frac{\partial}{\partial r}\left(r\frac{\partial p_c}{\partial r}\right) , \tag{3.4}$$

Overall mass uptake $M(t)$ is given by

$$\frac{dM}{dt} = \pi b^2 \ell \dot{Q} S_e (p_a - p_e) . \tag{3.5}$$

Boundary and initial conditions are

$$\begin{aligned} &p_e = p_c = p_o \quad \text{at} \quad t = 0 , \\ &p_e = p_c , \quad r = a . \end{aligned} \tag{3.6}$$

Transform to dimensionless variables defined by

$$\begin{aligned} &r' = r/a , \quad t' = \frac{D_c}{a^2} t , \\ &p_e' = \frac{p_e - p_o}{p_a - p_o} , \quad p_c' = \frac{p_c - p_o}{p_a - p_o} , \quad M' = \frac{M - M_o}{M_\infty - M_o} . \end{aligned} \tag{3.7}$$

where p_o is the initial inert gas partial pressure in the tissue and p_a the final (arterial) pressure, and

$$M_\infty - M_o = \{\pi(b^2 - a^2)\ell S_e + \pi a^2 \ell S_c\}(p_a - p_o) ,$$

M_o and M_∞ being the overall initial and final mass of inert gas in the tissue cylinder.

Equations (3.3) - (3.5) reduce to the following after ignoring the primes:

$$\frac{\partial p_e}{\partial t} = \lambda(1 - p_e) - 2\mu \left(\frac{\partial p_c}{\partial r}\right)_{r=1} , \tag{3.8}$$

where

$$\begin{aligned} \lambda &= \frac{\dot{Q}}{f}\frac{a^2}{D_c} = \frac{a^2/D_c}{1/\dot{Q}_e} \\ &= \frac{\text{Diffusion time scale in cellular region}}{\text{Perfusion time scale in extracellular region}} , \end{aligned} \tag{3.9}$$

$$\frac{\partial p_c}{\partial t} = \frac{1}{r}\frac{\partial}{\partial r}\left(r\frac{\partial p_c}{\partial r}\right) , \tag{3.10}$$

and

$$\frac{dM}{dt} = \frac{\lambda}{1+\mu}(1 - p_e) . \tag{3.11}$$

Boundary and initial conditions become

$$\begin{aligned} p_e = p_c &= 0 , \quad t = 0 \\ p_e = p_c &, \quad r = 1 . \end{aligned} \tag{3.12}$$

The Laplace Transform $\bar{F}(s) = \int_0^\infty e^{-st} F(t)dt$ is applied to the set of equations (3.8), (3.10), (3.11) and (3.12), yielding the following solutions:

$$\bar{p}_c = \bar{p}_e \frac{I_o(\sqrt{s}r)}{I_o(\sqrt{s})} ,$$

$$\bar{p}_e = \frac{\lambda}{s}\left(s + 2\mu\sqrt{s}\,\frac{I_1(\sqrt{s})}{I_o(\sqrt{s})} + \lambda\right)^{-1} , \tag{3.13}$$

$$\bar{M}(s) = \frac{\lambda}{s^2(1+\mu)}\left[1 - \lambda/\left(s + 2\mu\sqrt{s}\,\frac{I_1(\sqrt{s})}{I_o(\sqrt{s})} + \lambda\right)\right] .$$

where I_o and I_1 are the modified Bessel functions.

Once again, we are primarily interested in the inversion of $\bar{M}(s)$, which is straightforward by the calculus of residues.

The singularities are given by the points

$$s = 0 \quad \text{and} \quad s + 2\mu\sqrt{s}I_1(\sqrt{s})/I_o(\sqrt{s}) = -\lambda .$$

It is easily shown that the residue at the simple pole $s = 0$ is unity. Also it is known that the second set of singularities are all simple poles situated on the negative

real axis (see Appendix C). Thus writing $s = -\alpha_n^2$, then α_n is a root of

$$\alpha_n^2 + 2\mu\alpha_n \frac{J_1(\alpha_n)}{J_o(\alpha_n)} = \lambda \quad . \tag{3.14}$$

The residue is evaluated by standard methods and is

$$\frac{\lambda^2}{1+\mu} \frac{e^{-\alpha_n^2 t}}{\alpha_n^4} (1 + \mu + \mu J_1^2/J_o^2)^{-1} ,$$

hence

$$M(t) = 1 - \frac{\lambda^2}{1+\mu} \sum_{n=o}^{\infty} \frac{e^{-\alpha_n^2 t}}{\alpha_n^4(1 + \mu + \mu J_1^2(\alpha_n)/J_o^2(\alpha_n)} \quad . \tag{3.15}$$

3.3 Small Time Solution

The small time solution (i.e., $s \to \infty$) follows easily from (3.13) with the asymptotic approximation

$$\frac{I_1(\sqrt{s})}{I_o(\sqrt{s})} \sim 1 - \frac{1}{2\sqrt{s}} \quad .$$

Thus

$$\bar{M}(s) \sim \frac{\lambda}{1+\mu} \left(\frac{1}{s^2} - \frac{\lambda}{s^2(s + 2\mu\sqrt{s} + \lambda - \mu)}\right) \quad .$$

This function now has two real branch points, instead of a set of simple poles as in (3.13).

Thus expanding as a power series,

$$\bar{M}(s) \sim \frac{\lambda}{1+\mu} \left(\frac{1}{s^2} - \frac{\lambda}{s^3} + \frac{2\mu\lambda}{s^{7/2}} + \frac{\lambda(\lambda-\mu+4\mu^2)}{s^4} \quad \ldots\right) \quad .$$

If further terms are required, the asymptotic expansion of $I_1(\sqrt{s})/I_o(\sqrt{s})$ must be taken to the second order or higher.

Inverting term by term we have

$$M(t) \sim \frac{1}{1+\mu}\left(\lambda t - \frac{\lambda^2 t^2}{2} + \frac{16\mu}{15}\lambda^2\sqrt{\frac{t^5}{\pi}} + \right.$$

$$\left. + \lambda^2(\lambda - \mu + 4\mu^2)\frac{t^3}{6} \ldots\right) \qquad (3.15')$$

Notice that the first two terms are functions of λt which in terms of dimensional time become $\dot{Q}_e t$. Thus for very small values of time $M(t)$ depends only on the perfusion, as to be expected. As time increases the diffusion time scale begins to take effect and the perfusion diffusion interaction proceeds.

Note that, if $\mu \to 0$ thus implying zero cellular interaction, (3.15) with (3.14) reduces to the well-known perfusion controlled exponential solution

$$M(t) = 1 - e^{-\lambda t}$$

$$= 1 - e^{-Q_e t} \quad ,$$

where the time variable has been now replaced by its dimensional equivalent.

Also if $\lambda >> 1$ and $\mu \sim 1$, thus implying slow cellular diffusion compared with perfusion, a more realistic model of radial diffusion from a capillary into a cellular annulus might be more suitable. This case has been fully explored by Hills (1969b). However the present model is fully descriptive of this case and gives mass uptake effectively into a solid cylinder, the extracellular region being very rapidly equilibrated. It is known that diffusion into variously shaped solids are very similar if the basic parameters describing each geometry are slightly "adjusted".

In the case $\lambda << 1$, $\mu \sim 1$, implying fast cellular diffusion compared with perfusion, it is easily verified that a perfusion controlled single exponential response is again obtained as in the case $\mu \to 0$, though modified to include a now "fully stirred" cellular region.

Note that the case $\mu >> 1$ is not realistic simply because this implies that the tissue volume is almost entirely cellular, allowing very little space for gas input by perfusion. In any case blood and interstitial diffusion will be important as well and the assumptions in this paper are then invalid. One would need to treat this particular problem afresh as though perfusion is negligible. Hills (1969a) has considered this case. However the mathematical model proposed is open to question.

Thus it is seen that (3.14) and (3.15) adequately describe all known types of tissue structure, except in zones where the interstitial diffusion and blood perfusion time scales may be of comparable magnitude. In other words (3.14) may be used with confidence in determining the time constants of washout data from a fairly well-perfused tissue zone, irrespective of the tissue structure parameters.

3.4 Experimental Determination of the Parameters

It is expected that only the first three roots α_1 , α_2 and α_3 of (3.14) will be important in the overall response of gas uptake or elimination in the tissue zone chosen. Thus if three exponential time constants k_1 , k_2 and k_3 are extracted by backward projection of a washout curve, they will

satisfy the relation

$$k_i = \alpha_i^2 D_c/a^2 , \qquad (3.16)$$

where k_i is measured in dimensional units, usually min^{-1}.

Normally μ and D_c/a^2 are known from a separate experiment performed on an excised tissue sample. Hence the effective perfusion $\mathring{Q}$ can easily be solved from (3.9) and (3.14), providing the partition coefficient S_p, and hence f, is known.

On the other hand, since there are effectively three unknowns D_c/a^2, λ, μ and three equations (3.14), all three may be solved after elimination of α_i by means of (3.16). However this technique may lead to an unstable solution for the reason that (3.14) is sensitive to changes in λ. This means that if the perfusion $\mathring{Q}$ varies slightly in the course of an experiment, especially at initial stages, then solved numerical values of the parameters may be unreliable. Thus the former method is the best and is essentially similar to the procedure employed by Hills (1967).

Essentially the earlier time constants, k_2 and k_3, extracted by backward projection must be viewed with caution. The most reliable constant is obviously the asymptotic k_1, where it may be expected that conditions in the experiment have settled down to a stable state. Equation (3.14) will yield two other roots α_2 and α_3 and in turn predictions of k_2 and k_3 which may be compared directly with the actual values extracted by backward projection in order to gain some idea of the variation in the perfusion to the tissue at initial stages.

If the washout curve exhibits only one well-defined time-constant, thus implying $\mu \to 0$ in (3.14), then clearly perfusion dominates any cellular diffusion. However it seems impossible to derive any benefit from the attempted analysis of a washout curve applied to the whole body, covering a wide range of perfusion rates. Normally at least three time constants are found in such experiments. Whether these three values may be attributed to three well-defined perfusion controlled zones, or an overall interaction between a combination of perfusion and cellular diffusion controlled zones as supposed in this paper, cannot possibly be deduced from one overall washout curve.

If a washout curve for a well defined uniform tissue zone (such as a muscle) displays several time constants, then this provides the strongest evidence of perfusion and cellular diffusion interaction.

Table I shows data from Hills (1967) compared with data predicted by (3.14) in the case of washout of ^{85}Kr from rabbit muscle.

TABLE II

^{85}Kr Washout from Rabbit Muscle

(Data from Hills, 1967)

		Exp.	Calc.*	Exp.	Calc.*
Time constants (min)	1	86	(86)	197	(197)
	2	20.4	22.4	27.3	28.8
	3	6.7	8.0	6.5	8.2
Perfusion (ml/100 ml tissue per min)		1.45#	1.25	0.43#	0.40

* Values rounded off.

\# Hills values evaluated by considering the linearized capacity fraction of extracellular fluid rather than actual volume fraction f .

Equation (3.14) was solved by standard numerical methods available in Fortran Scientific Subroutines. Taking $\mu = 1.11$ and $D_c/a^2 = 0.00439 \times \sqrt{\frac{26}{85}} = 0.00243$ ($\sqrt{\frac{26}{85}}$ = Graham's Law correction from acetylene) taken from the previous chapter and assuming $S_p \sim 1$; i.e., $f = 0.47$, (3.14) was solved for λ and thence $\mathring{Q}$. The next two roots, as predicted, do not agree as closely as might be expected especially in the earliest

values. This is indicative of the basic inaccuracy of backward projection at small times, and the fact that the perfusion rate cannot be expected to be the same as that at the asymptotic stage after surgery and anaesthesia.

In the numerical solution of (3.14) it is confirmed that very small variations in the measured values of the earlier time constants give rise to a wide range of possible values of λ and thus $\mathring{Q}$. Strictly speaking the constants should be measured to at least 2 decimal places. Normally this is expimentally difficult to attain, and consequently only the asymptotic time constants can safely be used.

This, of course, immediately raises the question that since the assumption of full stirring is an essentially asymptotic approximation and that backward projection is an asymptotically orientated technique, then the interpretation of the solution for small times may be uncertain.

Unfortunately it is very difficult obtaining accurate data at small times. It seems clear however that unless better experimental methods are developed to accurately measure the washout (or uptake) curve at small times, one cannot really interpret λ and $\mathring{Q}$ reliably.

CHAPTER FOUR

A DIFFUSION MODEL OF THE DECOMPRESSION COMPUTER

4.1. Introduction

A method of simulating in real time the decompression format of a diver has been developed by the Canadian Forces Medical Service (Stubbs and Kidd, 1965) and has been successfully used in multilevel exposures to 60 m depth.

The instrument consists of four equal resistors in series (originally different resistors in parallel), through which inert gas flows, supposedly matching gas uptake and elimination in living tissues at hyperbaric environments. A mathematical analysis of the gas flow characteristics of the resistors has been given by Weaver and Stubbs (1968) and agrees well with experimental data.

Much emphasis has been attributed to the non-linear behaviour of the computer, in its undoubted success in predicting safe dive formats especially of a repetitive nature (Kidd et al, 1969, 1970). Therefore the question arises whether the computer is at all matched with existing mathematical models of gas uptake in tissue.

If one accepts that bulk diffusion into cellular material controls gas uptake in tissue necessary for predicting a decompression format, then it is of interest to know the relative importance of the non-linear aspects of the instrument and in particular its overall time scale. In this chapter we will prove that in fact the time scale of the instrument is of the same order of magnitude as that calculated in chapter II. To do this we must convert the semi empirical equations of the

instrument to an equivalent bulk diffusion model.

4.2 The Analogue

The gas mixture that is supplied to the diver is also fed to the analogue and begins flowing through the first resistor into a chamber, and thence through a series of three more resistors and chambers. The pressure in each cavity is metered by a bourdon tube gauge.

A decompression format is achieved by the diver himself controlling the highest pressure of the four chambers, in such a way as to ensure that this peak tension never exceeds a constant times the ambient pressure.

Gas flow in each resistor is essentially governed by 'slip flow', where the length of the free path of a molecule is comparable with the typical pore diameter of the resistor (~50 nm).

The equations of flow take the form (Weaver, Kuehn and Stubbs, 1968)

$$\frac{dp_i}{dt} = - A \left[(p_i - p_{i-1})(p_{i-1} + p_i + B) - (p_{i+1} - p_i)(p_i + p_{i+1} + B) \right] \ldots \qquad (4.1)$$

$$i = 1,2,3,4.$$

where p_i is the pressure in the i^{th} chamber and $p_o = P_A$ the external ambient pressure, and $p_5 = p_4$.

Typical values of A and B for air or nitrogen were determined empirically, in the region of

$$A = 1.8 \times 10^{-4} \text{ min}^{-1}$$
$$B = 120 \text{ p.s.i.a.}$$

The above equations are non-linear and this effect will become increasingly noticeable the greater the pressure.

Now to simulate a bulk diffusion system, an analogue is required which obeys Fick's Law, viz: the mass flux is proportional to the diffusion coefficient (D) times the gradient of the gas density (or concentration). This law in conjunction with a mass balance equation leads to the partial differential equation (Crank, 1956)

$$\frac{\partial p}{\partial t} = \frac{\partial}{\partial x} \left(D \frac{\partial p}{\partial x} \right) , \qquad (4.2)$$

where p is the pressure after time t at a point x, and x is measured in the direction of flow from one end of the slab of material, assuming uni-directional flow.

Suppose that (4.2) is split up into a finite difference scheme. If a four compartment array is employed, then it is necessary to determine the form of D such that (4.2) reduces to (4.1).

It is easily verified below that the appropriate form of D is

$$D = \frac{AL^2}{16} (2p + B) \qquad (4.3)$$

where L is the thickness of the material in the gas resistors.

Using this form of D, (4.2) can now be rewritten in a more appropriate form for finite differences as

$$\frac{\partial p}{\partial t} = \frac{L^2 A}{16} \frac{\partial^2 p^2}{\partial x^2} + \frac{L^2 AB}{16} \frac{\partial^2 p}{\partial x^2} .$$

Standard finite differences on the above equation yield

$$\frac{dp}{dt} = A(p_{i+1}^2 - 2p_i^2 + p_{i-1}^2) + AB(p_{i+1} - 2p_i + p_{i-1})$$

and (4.1) is quickly recovered on rearrangement of the latter.

Thus the pneumatic computer is essentially a finite difference approximation of the bulk diffusion equation into a slab of material, where the diffusion coefficient is a linear function of pressure, given by (4.3).

This means that we need merely calculate a characteristic value of D to make a comparison of the cellular diffusion time scale.

Before we do this, it is advisable to discuss this particular form of the diffusion coefficient as predicated by the pneumatic analogue. (Assuming for the moment that this is the correct mathematical model of gas uptake in tissue).

Whether the gas diffusion coefficient in cellular material actually varies with pressure in a similar manner to (4.3) is at present unknown. It is of course possible that at very high pressures, the diffusion coefficient may be an increasing function of pressure, in which case gas uptake, will be more rapid than elimination. This form of asymmetry has been noted by Hempleman (1957) and Eaton (1970). Their explanation that bubble formation and expansion on ascent interferes with gas elimination is, if correct, a much more dominant reason for asymmetrical behaviour than the likely variation of the diffusion coefficient in the small range of pressures considered.

However at ultra-high pressures in the region of 40 atmospheres, it is very likely that not only the diffusion coefficient but also the solubility of the inert gas will vary with pressure. The behaviour of the inert gas at these pressures will need to be known precisely in order to optimize decompression formats.

4.3 The Diffusion Time Scale

We determine the numerical values of D for the pneumatic computer using the typical empirical values of A and B. The computer has been thoroughly tested in the range 0 to 60 m, and the pressure p varies from 15 to 100 psi; thus from (4.3) it is found that

$$.00169 \lesssim D/L^2 \lesssim .00360 \text{ min}^{-1}$$

Compare these values with Hempleman's (1969) linear diffusion model value of $.00321 \text{ min}^{-1}$ and Hills (1969) averaged radial diffusion model value of $.00516 \text{ min}^{-1}$. See Table I for a more detailed comparison. Thus the pneumatic computer's time scale is generally longer than that of straightforward diffusion models of inert gas transport and only approaches current values at the greater depth zones.

The value of L is unknown, but may be assumed to be of the order of the semi-diameter of a typical tissue cell (15.0 μm); then D lies in the range

$$0.6 \times 10^{-10} \lesssim D \lesssim 1.4 \times 10^{-10} \text{ cm}^2 \text{ sec}^{-1},$$

somewhat less than the value $1.6 \times 10^{-10} \text{ cm}^2 \text{ sec}^{-1}$ for nitrogen in cytoplasm, as calculated from the mathematical analysis of chapter II.

The fact that the pneumatic computer has successfully achieved a large variety of safe decompression formats, whilst using a longer diffusion time scale than current models, may be attributed to its inherent asymmetry.

Thus since gas uptake is slower than the constant diffusion coefficient models and in turn uptake faster than

elimination, the combined effect appears to be such that it agrees well with linear models.

The fact that the linear bulk diffusion equation appears to provide an incomplete model for decompression formats has been indicated by Hempleman (1969). Here it was found necessary to lower the 'critical ratio' on long deep dives, which may of course have a number of explanations including bubble interaction.

However the pneumatic computer uses one single ascent ratio, based on the peak tension of any one of its four chambers. Whilst seeking the peak tension may be thought as effectively using a variable ratio, it should be noted that the gas flow is markedly non-linear on long deep dives (Stubbs and Weaver 1968).

Thus the position appears confusing especially as Eaton (1970) has suggested that there is no unique ascent path to the surface

In fact, it may be supposed that the basic parameters and critical ratio used in the computer may be just an optimum combination, approximating to a particular safe decompression format in the range 0-60 m .

It should be pointed out that the pneumatic computer only uses four compartments to what now appears to be essentially a numerical finite difference approximation to the bulk diffusion equation. Normally at least eight compartments should be used for accuracy. Hills (1967a) for example takes 27 compartments to fit the radial diffusion equation.

Thus it may be surmised that any extension of the present computer to as many compartments may be difficult because the non-linear effects of the compressible gas may tend to dominate undesirably. It seems unlikely that gas flow through porous resistors is an appropriate mathematical model to simulate diffusion in tissue, simply because the flow is not necessarily an isothermal or Poisieulle flow at hyperbaric exposures.

If in fact actual gas uptake in tissue is governed by a diffusion coefficient which is some function of pressure, then clearly any pneumatic analogue will eventually deviate from the true situation, unless it matches faithfully the precise non-linear diffusion law in tissue.

The important experiment of determining the dependence (if any) of the cellular diffusion coefficient and solubility on pressure at ultra depths remains to be carried out.

In the meantime, it is much simpler to use a constant valued diffusion coefficient to model gas transport, and to rather adjust the tissue geometry parameters to attempt a fit of experimental data.

In conclusion, it is remarkable that after a number of purely empirical designs of series-parallel combinations of resistors and human decompression trials, the most successful instrument developed turns out to be a mathematical model of diffusion with a time scale similar to that of intracellular transport.

This fact alone offers the strongest evidence that linear

bulk diffusion into the cellular phase of tissue is the main mode of uptake of inert gas for computing safe decompression formats from a hyperbaric environment.

However in the next chapter we discuss the case where the interaction of perfusion and diffusion in a homogeneous tissue may become important.

CHAPTER FIVE

THE INTERACTION OF DIFFUSION AND PERFUSION IN HOMOGENEOUS TISSUE

5.1 Background

For many years there has been some doubt as to whether diffusion or perfusion is the dominant mechanism for uptake of inert gas in tissue.

A number of different mathematical models have been proposed, beginning with Zuntz (1897), von Schrotter (1906) and Haldane (1908). All these are similar and were based upon perfusion being the dominant mechanism. Haldane was the first to introduce the concept of a tissue half-saturation-time, which is defined to be that time for a tissue to receive one half the nett uptake of gas after a sudden change in arterial gas pressure. In this way various tissues become characterized by their half-times. For the rest of this chapter, therefore, the early perfusion approach will be referred to as the Haldane model.

The most comprehensive review of early papers is that of Kety (1951), and since then a number of papers have appeared.

Perhaps the most important recent review is that of Hills (1970 c) who in a remarkable paper shows that much of the present experimental data can be equally well correlated by a diffusion or perfusion theory approach. In fact it seems that perfusion and diffusion mechanics are inextricably intertwined. The purpose of the chapter will be to highlight this interaction and to define the conditions from a fundamental viewpoint.

The main features of all these models of gas transport

through tissue appear to be a combination of some of the following dominant aspects

(i) perfusion,
(ii) bulk diffusion,
(iii) fully transient,
(iv) axial as well as radial concentration dependence along capillary.

To a lesser extent additional features are present, and include a capillary permeability term (often used in place of true bulk diffusion) and anisotropy (diffusion velocity different in radial and axial directions).

Papers concerned with the uptake of a substance other than an inert gas introduce a number of other assumptions and boundary conditions, which will not be considered here.

Of the more recent papers concerned with gas transport through tissue, a number have appeared which all attempt to include some of the features (i) to (iv) above. These include Schmidt (1952, 53), Thews (1953), Blum (1960), and Hills (1970 b). The most important paper prior to 1951 is probably that of Morales and Smith (1948), being the final paper in a set of six covering various models and approaches (1944-1948).

Schmidt and the latter authors (except Hills) attempt to treat (i), (iii) and (iv) but instead of (ii) use a capillary membrane property which is a first order approximation to bulk diffusion in the case of an inert gas. Table III gives a brief summary of recent approaches, most of which include an approximation to the axial dependent term (iv). Some are concerned with substances other than inert gases, but are included for interest.

However in nearly all these earlier papers, no attempt has been made to extract and compare the crucial parameters from the mathematical model, viz: vascularity index, perfusion time scale and the diffusion time scale.

The most common approximation is to the bulk diffusion term, where gradients are simply replaced by their first order approximation, that is, the linear difference between two nearby concentrations divided by the distance between them. As Hills (1970 b) has shown it is usually a poor approximation at small to medium times.

In some cases, the model is assumed non-transient. Whilst this approach is reasonable for experiments which may be slowly varying, and/or of short duration, considerable errors will occur over saturation times.

At this stage it is perhaps pertinent to offer some justification for the emphasis on axial dependence, as shown in the first part of Table III. First of all there is no intuitive reason for omitting axial dependence in preference to bulk diffusion or perfusion. To see this, consider a long straight capillary surrounded by a tissue annulus. If the blood flow along the capillary is very fast, then one would expect that diffusion into the tissue would be the limiting factor, because the wall of the capillary would be effectively at uniform arterial inert gas pressure. In this case, axial dependence is negligible.

TABLE III

SUMMARY OF VARIOUS MATHEMATICAL MODELS

OF TRANSPORT IN TISSUE

	(i) Perf-usion	(ii) Bulk Diff-usion	(iii) Fully Trans-ient	(iv) Axial Depemd-ence.
Morales and Smith (1948)	Yes	1st Order	Yes	1st Order
Schmidt (1952, 53)	"	"	"	Yes
Sangren and Sheppard (1953)	"	"	"	"
Thews (1953)	No	Yes	No	"
Blum (1960)	"	1st Order	"	"
Bellman, Jacquez and Kalaba (1960)	Yes	"	Yes	"
Hills (1970 b)	1st Order	Yes	No	"
Haldane (1908)	Yes	No	Yes	No
Teorell (1937)	No	Yes	"	"
Roughton (1952)	"	"	"	"
Morales and Smith (1944-45)	Yes	1st Order	"	"
Harris and Burn (1949)	No	Yes	"	"
Hills (1969 c)	"	"	"	"
Hills (1967 b)	"	"	Asy-mpt.	"
Hennessy (1971 b)(Chap. 3)	Yes	"	Yes	"

Note: not all models employ the same boundary conditions.

If on the other hand, blood flow is very slow, then linear perfusion becomes the limiting mechanism, because one can now imagine that the tissue will absorb all the gas in the capillary leaving a zero concentration at the exit. Here once again, axial dependence falls away when considering the overall uptake of the tissue (which would be simply a linear growth rate). Clearly then between these two extremes, there may be a situation where diffusion and perfusion interact and the length of the capillary then becomes important.

On heuristic grounds alone it seems reasonable to expect that the typical length of a capillary is attributable to some dependence on its gas transport properties. If the capillary length does not appear directly in the model, then it implies that the capillary is simply being treated as a point source of gas, in which case, spherical diffusion might just as well be invoked instead of cylindrical diffusion.

On the other hand, it may of course be possible that the capillary is indeed acting as a point source, by virtue of its length and distribution in the tissue.

In all the approximation shown in Table III there is hardly any rigorous justification for ignoring a term, based on an order of magnitude analysis. Of course in some cases no estimate of a physical quantity may be possible. In these situations, analysis of the order of magnitude of a term can often highlight an area of future experiment, and can also curtail the domain of validity of an existing model.

Thus the aim of this chapter is to focus attention on

tissue structures, where all four of the above features assume importance. In doing so, the role played by perfusion and diffusion in tissue is seen in a clearer light than perhaps hitherto. In any case, the literature does not appear to contain a non-firstorder mathematical model which attempts to incorporate bulk diffusion and axially dependent perfusion together, and to examine their interaction.

5.2 The Mathematical Model

Nearly all the models mentioned in section 5.1 propose a structure based upon a single straight capillary of given characteristic length (ℓ) , radius (a) , surrounded by a tissue annulus, of some realistic outer radius (b) . This approach dates back to Krogh (1919 b, c).

Studies of a particular tissue show that whilst a , b and ℓ all vary, they do so between definite limits. Therefore, there must exist a set of dimensions for a , b and ℓ which characterize that particular tissue under a given metabolic state. Changing the latter may cause a and b to vary by opening up non-active capillaries, for example.

On the other hand it is noticed that capillaries are situated in an apparently random manner, where the end of one capillary may be placed near the beginning of another. Thus it may even be parallel to it. For example Schmidt (1952) uses this argument to dispense with the axial extra-cellular concentration gradient.

Thus the question arises : how does one justify allocating a typical tissue radius or length of capillary. It seems

that the answer must be simply that there is at present no better tractable approach. In any case each capillary has to serve a definite volume of tissue in its immediate neighbourhood; we merely specify it to be a circular cylindrical annulus on grounds of mathematical convenience, and its apparent closeness to physical reality in specific tissues such as muscle. Contrast this approach with chapter 3 where we supposed the extra-vascular space to be a solid cylindrical space, with no direct reference to the capillary structure. However in this chapter we make an attempt to relate the capillary dimensions with actual observation in tissue. (Krogh 1919 b).

Moreover, as Gonzalez-Fernandez and Atta (1972) have shown, negligible error is made by choosing a circular cylindrical annulus in preference to a hexagon of equal area cross-section. Larger errors can occur if square or triangular tissue structures are present. In these cases, the cylinder must be considered a first approximation.

It is now necessary to describe the extra capillary space from the point of view of a diffusion medium. If this space is purely interstitial then diffusion will be very rapid (about a 1 second saturation time) as Roughton (1952) has shown. If of course the tissue has a low vascularity index α(= a/b), then the saturation time rises considerably, but still well away from the very large times known to exist. On the other hand, as we have seen in chapter 2, the tissue is actually a heterogeneous, diffusion medium since the diffusion coefficient is believed to be 10^4 times smaller in cytoplasm.

Because of this dominance for cellular diffusion, it seems reasonable to suppose that the interstitial space is effectively fully stirred. This was a basic assumption in chapter 3. However, we are then forced to give this space a precise volume in the tissue annulus, which will complicate the model considerably. To avoid this, we assume that the annular tissue cylinder is an entirely cellular space, as envisaged by Hills (1966). Any actual interstitial diffusion which may be present may be included in a heuristic sense by adjusting (reducing) the vascularity ratio α or the capillary length. If on the other hand the cellular content of the annulus is sparse, then an entirely new model must be reworked. In other words, we are assuming effectively that the inert gas capacity of the interstitial space is much less than the cellular content of the tissue annulus, a fact born out by observation in many tissues, for example skeletal muscle.

The outer boundary and sides of the annular cylinder are supposed impermeable by symmetry. It is not difficult to show that the effect of axial diffusion down the capillary is quite negligible compared with perfusion, Taylor (1954). Also, radial diffusion may be supposed 'instantaneous' compared to the other terms. Thus the blood is assumed to be a fully stirred fluid in the radial direction as it travels through the capillary. There is a continual loss of gas en route down the capillary and thus the concentration is axially dependent. Figure 3 describes the model with its main parameters.

We suppose that blood (taken to be a Newtonian fluid, for

purposes of defining a volume flux) flows uniformly through the capillary with velocity V. It carries an inert gas, whose arterial tension is fixed at p_a, derived from the exposure to the hyperbaric environment. Initially the region is at a tension p_o.

We denote the gas tension in the blood by $p_b(z, t)$ and in the cellular tissue $p_c(r, z, t)$. Notice that p_b only depends on z, because of rapid stirring in the r direction.

Applying a mass balance to a disc of fluid in the capillary and taking the limit, we obtain

$$\frac{\partial p_b}{\partial t} = - V \frac{\partial p_b}{\partial z} + \frac{2D_c S_p}{a} \left(\frac{\partial p_c}{\partial r}\right)_{r=a} \tag{5.1}$$

Also the diffusion equation holds in the celluar space

$$\frac{\partial p_c}{\partial t} = \frac{D_c}{r} \frac{\partial}{\partial r} \left(r \frac{\partial p_c}{\partial r}\right) + D_c \frac{\partial^2 p_c}{\partial z^2} \tag{5.2}$$

subject to

$$\frac{\partial p_c}{\partial r} = 0, \; r = b \; , \; 0 \leq z \leq \ell, \quad t \geq 0$$

$$\frac{\partial p_c}{\partial z} = 0, \; z = 0 \; , \; \ell, \; a \leq r \leq b \; , \quad t \geq 0$$

and

$$\left.\begin{aligned} & p_b = p_c \; , \; r = a \; , \; 0 \leq z \leq \ell. \\ & p_b = p_c = p_o \; , \; a \leq r \leq b \; , \; 0 \leq z \leq \ell, \; t = 0 \\ & p_b = p_a \; , \; z = 0 \; , \; t > 0 \; . \end{aligned}\right\} \tag{5.3}$$

The mass uptake of inert gas is given by

$$\frac{dM}{dt} = \pi a^2 V S_b \left(p_a - p_b(\ell, t)\right) \tag{5.4}$$

The average tissue gas tension is perhaps a more convenient variable than M, and is given by

$$p = M/(\pi a^2 \ell S_b + \pi(b^2 - a^2)\ell S_c) \tag{5.5}$$

and thus

$$\frac{dp}{dt} = \frac{V/\ell}{(1+\frac{(1-\alpha^2)}{\alpha^2}S_p)} \quad (p_a - p_b(\ell, t)) \tag{5.6}$$

where $\alpha = a/b$.

Notice that if V becomes very large, then $p_b(\ell, t) \to p_a$, which reduces to straight diffusion into the cellular annulus, and in the limit, using (5.1), we have

$$\frac{dp}{dt} = -\frac{2D_c}{a} \frac{S_p}{(1+\frac{1-\alpha^2}{\alpha^2} S_p)} \left(\frac{\partial p_c}{\partial r}\right)_{r=a} \tag{5.7}$$

This is essentially Hills (1966) equation for pure radial diffusion into an annulus and will only be valid for $V >> \ell$.

Transform to dimensionless variables as before:

$$r = br' \ , \quad z = \ell z' \ , \quad t = \frac{b^2}{D_c} t'$$

$$\frac{p_b - p_o}{p_a - p_o} = p_b' \qquad \frac{p_c - p_o}{p_a - p_o} = p_c' \tag{5.8}$$

$$\frac{p - p_o}{p_a - p_o} = p'$$

Substitute into (5.1), (5.2) and (5.6) to obtain

$$\frac{\partial p_b}{\partial t} = -\lambda \frac{\partial p_b}{\partial z} + \frac{2S_p}{\alpha} \left(\frac{\partial p_c}{\partial r}\right)_{r=a} \qquad 0 \leq z \leq 1 \ , \ t > 0 \tag{5.9}$$

where $\lambda = \dfrac{b^2/D_c}{\ell/V} = \dfrac{\text{Diffusion time scale in cells}}{\text{Perfusion time scale for capillary}}$

and $$\frac{\partial p_c}{\partial t} = \frac{1}{r}\frac{\partial}{\partial r}\left(r\frac{\partial p_c}{\partial r}\right) + \beta\frac{\partial^2 p_c}{\partial z^2} \qquad (5.10)$$

$$0 < \alpha \leq r \leq 1\ , \quad 0 \leq z \leq 1\ , \quad t > 0$$

where $\beta = b^2/\ell^2$.

Finally, we have

$$\frac{dp}{dt} = \frac{\lambda}{1+\mu}\left(1 - p_b(1\ ,\ t)\right) \qquad (5.11)$$

where $\mu = \dfrac{(1-\alpha^2)S_p}{\alpha^2} = \dfrac{\text{gas capacity of cells}}{\text{gas capacity of blood}}$.

Notice that we have used b rather than a to reduce r and t to dimensionless variables. This is because it is conceptually more appropriate to consider the diffusion time scale as b^2/D_c rather than a^2/D_c . The latter term is simply the diffusion time scale across the radius of a capillary which of course does not consist of cellular material. The quantity a^2/D_c must rather be regarded as a constant physical parameter of the tissue structure (because it is known that a varies only slightly in a given tissue under different conditions of stress.) On the other hand b^2/D_c is the diffusion time scale of the tissue and is a measure of the time for diffusion processes to occur in the extra-vascular cellular space normal to the capillary.

If V is large, than $\lambda >> 1$ and (5.11) will become in the limit the dimensionless equivalent of (5.7),

$$\frac{dp}{dt} = \frac{-2S_p}{\alpha(1+\mu)}\left(\frac{\partial p_c}{\partial r}\right)_{r=\alpha} \qquad (5.12)$$

Consider the parameter $\beta = b^2/\ell^2$. Typical values of b are 15 - 30 μm , whereas ℓ is normally .4 to 1 mm (Krogh, 1936).

Thus $\beta < .005$, and so the last term on the right hand side of (5.10) may be ignored, over a wide range of vascularities, providing always that the tissue remains a homogeneous and purely cellular.

The boundary conditions become

$$\begin{aligned} &\frac{\partial p_c}{\partial r} = 0, \quad r = 1, \quad 0 \leq z \leq 1 , \quad t \geq 0 \\ &p_b = p_c, \quad r = \alpha , \quad 0 \leq z \leq 1 \\ &p_b = p_c = 0, \alpha \leq r \leq 1 , 0 \leq z \leq 1 , \quad t = 0 \\ &p_b = 1, \quad z = 0 , \quad r = \alpha , \quad t > 0 \end{aligned} \tag{5.13}$$

Notice that we must relax the condition

$\frac{\partial p_c}{\partial z} = 0$ on $z = 0 , 1 , \alpha \leq r \leq 1 , t \geq 0$, since otherwise the equations (5.9), (5.10) become overdetermined. The reason for this is that since the z dependence has been removed from (5.10), it is no longer possible to specify a zero gradient at $z = 0 , 1$. On the other hand the problem is still z dependent by virtue of (5.9) and (5.13). Thus $(\frac{\partial p_c}{\partial z})_{z=0,1}$ will in general be non-zero, thereby implying a loss of gas from each end. However this loss is quite negligible, as can be seen by inspecting the dimensionless mass flux from one face in the worst case:

$$\frac{b^2}{\ell^2} \underset{\alpha \leq r \leq 1}{\text{Max}} \left(\frac{\partial p_c}{\partial z}\right)_{z=0,1} \leq \beta$$

which has been supposed $< < 1$.

The Lapace Transform is applied to the set of equations (5.9), (5.10), (5.11) and the boundary conditions (5.13). Solution is straightforward with the results set out in the following form:

$$\bar{p}_b(z,s) = \frac{1}{s} \exp\{-\frac{sz}{\lambda}(1 - \frac{2S_p}{\alpha\sqrt{s}} \frac{f(\alpha,s)}{g(\alpha,s)})\} \quad , \tag{5.14}$$

$$\bar{p}_t(r,z,s) = \bar{p}_b(s) \quad g(r,s)/g(\alpha,s) \quad , \tag{5.15}$$

and

$$\bar{p}(s) = \frac{\lambda}{1+\mu} \quad (1 - s\bar{p}_b(1, s))/s^2 \tag{5.16}$$

where the functions f and g are defined as

$$\begin{aligned} f(r,s) &= I_1(r\sqrt{s})\, K_1(\sqrt{s}) - I_1(\sqrt{s})\, K_1(r\sqrt{s}) \\ g(r,s) &= I_o(r\sqrt{s})\, K_1(\sqrt{s}) + I_1(\sqrt{s})\, K_o(r\sqrt{s}) \end{aligned} \tag{5.17}$$

K is the modified Bessel function of the second kind. We are of course primarily interested in evaluating the average inert gas pressure of the tissue region given by (5.16). Unfortunately inversion of this function analytically is not possible, because the singularities are isolated essential and the residue cannot be obtained in terms of recognizable functions. This can be seen by attempting to form the Laurent expansion at the singularity points given by

$$g(\alpha,s) = 0 \ .$$

[In fact this point can be considerably clarified by first attempting to find the inversion of the simple function $\frac{e^{1/4s}}{s}$. There is only one singularity at the point $s = 0$, and thus the residue is simply the coefficient of $1/s$ in the expansion of $\frac{e^{st+1/4s}}{s}$ about $s = 0$. It is easy

to show that this turns out to be $I_o(\sqrt{t})$ by inspection of the resulting series. Now consider the task of performing the same operation on a function such as

$$\frac{e^{f(s)/s}}{s}$$

where $f(s)$ is a regular function everywhere, $f(0) \neq 0$.

It is soon seen that it is simply not feasible to invert the function by the Laurent series technique.]

Thus a numerical inversion technique must be employed to invert (5.16).

5.3 The Perfusion Approach

At this stage it is of interest to show how the Haldane Perfusion dominated approach can be deduced from the present model. The basic step is to assume that diffusion is unimportant in the extra-vascular space (assuming an 'aqueous' $D \sim 10^{-5}$ cm^2/sec). This is another way of stating that the diffusion time scale is very much less than the perfusion time scale, or $\lambda << 1$. This is effectively assuming the entire extra-vascular space to be fully stirred, which only approaches this condition at large times. This implies that the blood leaves the tissue in equilibrium with the mean tissue inert gas pressure. This latter form was first used by Zuntz (1897) and has since formed the basis of all perfusion theories.

Using this, equation (5.11) can be considerably simplified to read

$$\frac{dp}{dt} = \frac{\lambda}{1+\mu} (1 - p) \qquad (5.18)$$

which on integration, using the boundary conditions, we obtain

$$p = 1 - e^{-\lambda t/1+\mu}$$

which may be re-interpreted in terms of dimensional variables to read

$$p = p_a - (p_a - p_o)e^{-kt} \qquad (5.19)$$

where $k = \dfrac{V}{\ell(1+\mu)} = \dfrac{P}{\alpha^2+(1-\alpha^2)S_p}$

where P in the blood perfusion, i.e. the volume of blood entering the tissue per unit volume of tissue per minute. Thus

$$P = \frac{\pi a^2 V}{\pi b^2 \ell} = \alpha^2 V/\ell \qquad (5.20)$$

In the case where $S_p \simeq 1$, k reduces to P. Equation (5.19) is the well known Haldane equation which gives a tissue half time T_H

$$T_H = \frac{(\alpha^2+(1-\alpha^2)S_p)\log 2}{P} \quad \text{minutes} \qquad (5.21)$$

The literature normally quotes $T_H = \log 2/P$ where $S_p = 1$ has been assumed. In any case even for lipids, where $S_p \simeq 5$, little error is made if α is small. Only in very vascular tissue is there an appreciable difference. Thus the Haldane approach yields two important parameters, the tissue half-time T_H and the blood perfusion P. If the present model is to be contrasted with the perfusion approach, it should relate these two parameters and compare it to the relationship of (5.21).

It is worthwhile examining in closer detail the meaning of the approximation that the blood leaves the tissue in

equilibrium with the average pressure. First of all, as has been noted, this is only likely to be approximately true at large times. The rate of change of the average tissue pressure is given by (5.11). Compare this with the rate given by (5.18). It is clear that since $p > p_b(1,t)$ for all t, then the actual rate of increase of the average pressure will always be less than the Haldane rate, becoming closer as the time grows large. This in turn means that the Haldane half-time is in fact an over-estimate of the actual tissue half-time, other things being equal (such as perfusion vascularity, diffusion time scale etc). This fact can be clearly seen in the numerical solutions in chapter six.

5.4 The Diffusion Approach

In contrast to the perfusion theory above, the diffusion approach is based on the assumption that the diffusion time scale is a non-negligible entity in the extra-vascular space. That is, the diffusion coefficient is very much smaller in the cellular space. This of course is an incomplete assumption because the perfusion time scale may also be non-negligible. One must state that $\lambda >> 1$. Effectively one is assuming that the blood velocity is so fast that the capillary wall is instantly exposed to the full arterial input gas pressure. Proceeding with this assumption, one easily solves the radial diffusion equation into an annular cylinder (Hills, 1966).

This solution is also present in our model, and can be got by simply letting $\lambda \to \infty$ in (5.14), (5.15) and (5.16).

The result for $\lambda \to \infty$ is

$$\bar{p}(s) = \left(1 - \frac{2}{\alpha}\frac{S_p}{\sqrt{s}}\frac{f(s,\alpha)}{g(s,\alpha)}\right) \Big/ (1+\mu)s.$$

which can be inverted by standard methods, and after some labour, yields

$$p(t) = \frac{1}{1+\mu} + \frac{\mu}{1+\mu}\left\{1 - \frac{4}{1-\alpha^2}\sum_{n=1}^{\infty}\frac{e^{-\beta_n^2 t}}{\beta_n^2}\left[\frac{J_o^2(\alpha\beta_n)}{J_1^2(\beta_n)} - 1\right]^{-1}\right\} \quad (5.22)$$

where β_n are the roots of

$$J_o(\alpha\beta)\, Y_1(\beta) - Y_o(\alpha\beta)\, J_1(\beta) = 0 . \quad (5.23)$$

Notice that according to our general definition, the average pressure is that of the <u>whole</u> space, both intra and extra-vascular, whereas Hills definition for the total uptake considers only the extra-vascular space. In other words, he ignores the quantity of gas present in the capillary. Naturally in tissue of small vascularity, this omission is negligible. Thus as $\mu \to \infty$, p approaches the standard result for the average pressure in the annulus. (This is the term in brackets in (5.22)). This latter term has been used successfully by Hills (1966) as a model of gas uptake in tissue in correlating decompression formats. The value for μ in this model was about 25 and thus a small error of .04 is made in the average pressure term.

5.5 <u>The Perfusion-Diffusion Interaction</u>

Thus it is seen that the present model actually contains as subcases the Haldane perfusion model and the Hills annular diffusion model. In other words, by solving (5.16), using

realistic values of the vascularity α , the diffusion time scale a^2/D_c and the blood perfusion P , the complete interaction may be observed and discussed in the light of the two extreme forms of the model, viz: diffusion versus blood perfusion.

It should be noted that the model proposed in chapter three also attempted to highlight this interaction. In that chapter though, the entire extra-cellular region was assumed to be fully stirred, an assumption which has been avoided in this chapter by assuming (i) purely cellular extra-vascular space, and (ii) an axially dependent gas distribution. In addition the present model is more realistic, taking into account radial diffusion from a capillary (as well as axial dependence).

In Figure 4 are shown the Haldane and Hills curves of Half Time plotted against perfusion on Log-log paper.

By (5.21), the Haldane curve should be a constant line of slope -45° , for $S_p \simeq 1$. On the other hand, the Hills half time is independent of the blood perfusion and are thus horizontal lines, where the ordinate intercept depends of course on the vascularity α . Clearly there will be zones where the perfusion P is very low, in which case the Haldane Half-time >> Hills Half-time, and vice versa for large P .

The numerical solution of (5.16) may be expected to take up a curve which moves smoothly from the Haldane to the Hills curve as P is increased. The interesting issue is over which range of P is the interaction most predominant. In section 6.4, this question will be fully answered, and the main

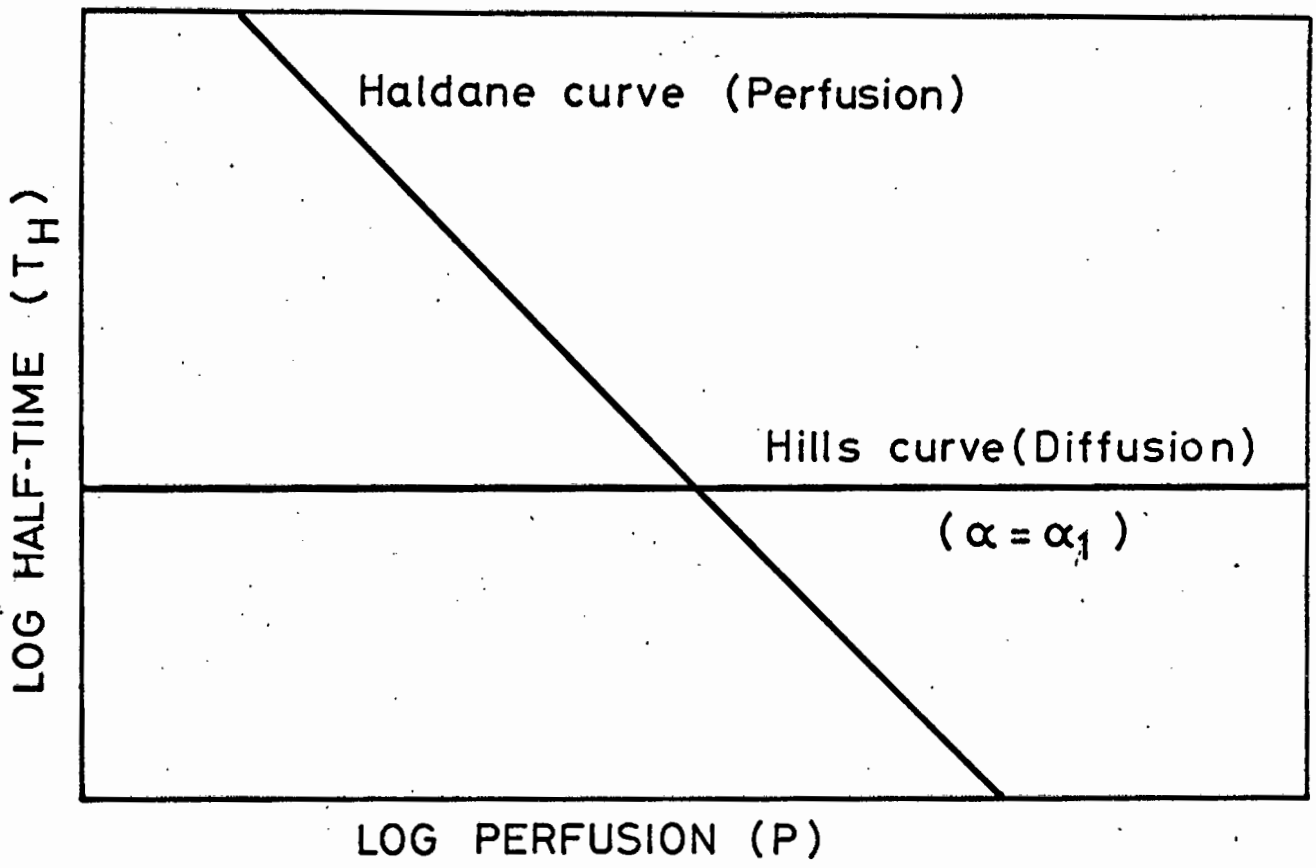

FIG.4 TYPICAL HALF-TIME CURVES IN DIFFUSION / PERFUSION THEORIES

results confirm in a positive manner that neither diffusion nor perfusion may be singled out as the dominant mode of uptake.

5.6 Large Time Solution

It is of interest to attempt to obtain the large time solution of (5.16) in the hope that a dominant asymptotic exponential component may be extracted. However a lengthy analysis and considerable manipulation of the function $f(r,s)$, $g(r,s)$ for small s proved disappointing. The best that could be done was to show that the average pressure has an exponential behaviour at large times, where the time constant k was the same as in the Haldane equation (5.19). However the coefficient in front of the exponential could not be evaluated with any certainty (we expect it to be at least greater than the Haldane coefficient of unity). The details are omitted here owing to the inconclusive results. In any case the numerical inversion takes care of this difficulty with apparent ease.

5.7 Small Time Solution

The next step would be to inspect (5.16) for large s, i.e. small time. Once again there is considerable labour for the results obtained. The asymptotic expansions for $I_{o,1}$ and $K_{o,1}$ are taken from Abramovitz and Stegun (1965) and a first order approximation is carried out. The result is

$$\bar{p}(s) \sim \frac{\lambda}{s^2(1+\mu)} \left(1 - e^{-S_p/\lambda\alpha^2} \exp\left(- \left({}^{s}/_{\lambda} + \frac{2S_p\sqrt{s}}{\alpha\lambda}\right)\right)\right) \qquad (5.24)$$

This function can be inverted analytically without difficulty. On a close examination it will be seen that the expression contains the small time solution when the model is perfusion controlled ($\lambda << 1$) and also the small time solution if diffusion dominates ($\lambda >> 1$) . This can be seen by considering the term $e^{-S_p/\lambda\alpha^2}$. For $\lambda << 1$, the exponential becomes very small, and the small time solution degenerates to a linear uptake of gas as to be expected. For $\lambda >> 1$, the exponential approaches unity, and a little manipulation reveals the standard small time solution into the annulus, (Carslaw & Jaeger, 1959), plus a correction for the uptake in the capillary itself. For intermediate values ($\lambda \sim 1$), the solution is effectively a balanced combination of the perfusion and diffusion solutions. However, in the numerical solutions of section 6.4, this function was not inverted as a check against the analytical inversion of (5.24), because the method of inversion was well established and also that the half time solution was required.

Instead it was found more convenient to compare as a "check" the Haldane half time and the Hills half time with the numerical inversion of (5.16).

5.8 Concluding Remarks

Under the various assumptions and conditions, we have solved the problem of uniform flow of blood carrying an inert gas entering a region of tissue via a long capillary. We have assumed that the extra-vascular space is entirely cellular, where a very long diffusion time scale exists.

This was done to highlight the perfusion/diffusion interaction, since the diffusion time scale in extra-cellular space is very short (a few milli seconds compared with the cellular diffusion time scale of a few minutes).

To see that the axial dependence is an important aspect of the problem, consider a magnified model x 1000 of the capillary structure. This would be the equivalent of a material cylinder about 1 metre long, 5 cm diameter served by a central tube about 1 cm in diameter. It is known that the maximum velocity in the capillary is about 1 mm sec^{-1} , and thus in the model a fluid velocity of at most 1m sec^{-1} would be imposed. The diffusion coefficient would be of order $10^{6} \times 2 \times 10^{-10}$ $= 2 \times 10^{-4}$ cm^{2} sec^{-1} , similar to that in water. With this model in mind, it can be appreciated that depending on the flow velocity (which can be made very low by the pre-capillary sphincters), an entire spectrum of behaviour can be expected ranging from a linear uptake to straight annular diffusion. The interesting feature of the present model is a complex feed-back effect as the gas diffuses into the annulus near the arterial end. As saturation progresses, the capillary gas tension will be depleted less and more gas will become available to saturate zones further downstream.

In section 6.4, the full implications of the model will be seen when perfusion is contrasted with diffusion over a wide range of realistic values of the blood perfusion P .

CHAPTER SIX

NUMERICAL INVERSION STUDIES

6.1 Introduction

In this chapter we construct numerical inversions of the Laplace transform solutions to the mathematical models discussed in chapters 2, 3 and 5 . In each case a fairly complicated function involving modified Bessel functions requires inversion. All calculations are done in double precision as detailed in Appendix A and B.

To judge a particular inversion method for accuracy is very difficult. The best that can be done at present is to (i) compare different inversion methods (ii) compare different orders of approximation of the quadrature formula in a given method (iii) compare the numerical solution with the small and large time analytical solution in cases where this is possible or meaningful, and (iv) to compare the numerical solution to the full analytical solution even if this can be only obtained in special restricted cases.

A combination of these checks can lead to a reasonable numerical solution of the problem. Note however that the solution is only as good as the empirical data used to verify the mathematical model. Since measurements in the biological sphere are subjected to considerable experimental 'noise'. highly accurate numerical solutions may be unnecessary, and possibly misleading.

Unfortunately there is often a wide variation in the results between different inversion methods. It usually depends on the quadrature formula used to represent the Laplace

Transform. This in turn depends on how well the actual Laplace Transform function is approximated by polynomial or other methods.

Broadly speaking there are good inversion formulae for oscillatory inverse Laplace transforms, which are usually bad for momotone functions consisting of a combination of exponential terms. The same applies vice versa. Thus if one knows at the outset the likely shape of the inverse Laplace Transform (that is, oscillatory or monotone multi exponential) one can then choose an appropriate inversion formula. In this thesis we are primarily concerned with the mass uptake of inert gas $M(t)$ in tissue at hyperbaric exposure. In all cases $M(t)$ is a monotone increasing function which reduces to a sum of exponential terms in special cases. This suggests that we employ the inversion method of Bellman, Kalaba and Lockett (1966) and Norden (1961), which have been successfully used on similar functions. Unfortunately these methods are not continuous in time and had to be modified [see Appendix A] .

Recently Piessens (1972) has presented a numerical inversion method which claims ultra-high accuracy. The examples he chose are oscillatory on the t plane ($J_o(t)$ and $\cos\sqrt{t}/\sqrt{t}$), and thus it should not be surprising if the method yields indifferent results for monotone functions. This is confirmed in the numerical experiments below.

In all cases μ is set equal to 1.11 as determined from chapter 2. Only the value of λ is allowed to vary as

described in the following models. All computing was performed on the University of Cape Town Univac 1106 computer.

6.2 Numerical Solution for Excised Tissue

We recall the Laplace Transform $\bar{M}(s)$ given by (2.15)

$$\left.\begin{aligned} \bar{M}(s) &= \frac{\lambda}{1+\mu}\,\frac{\sqrt{\theta}}{s^2}\,\tanh\sqrt{\theta} \\ \text{where} \\ \lambda\theta &= s + 2\mu\sqrt{s}\; I_1(\sqrt{s})/I_0(\sqrt{s}) \end{aligned}\right\} \qquad (6.1)$$

and where λ is the ratio of cellular to extracellular diffusion time scale.

The small time solution to the first order from (2.22) is

$$M_s = \frac{\sqrt{\lambda}}{1+\mu}\left(2\sqrt{\frac{t}{\pi}} + \mu t - \frac{2}{3}\,\mu(1+\mu)\,\frac{t^{3/2}}{\sqrt{\pi}}\right), \qquad (6.2)$$

whilst the large time solution (2.20) is

$$M_\ell = 1 - Ae^{-\alpha^2 t}, \qquad (6.3)$$

where α is the smallest root of

$$\alpha^2 + 2\mu\alpha\; J_1(\alpha)/J_0(\alpha) = \pi^2\lambda/4 . \qquad (6.4)$$

and

$$A = \frac{\pi^2\lambda^2}{2(1+\mu)} \Big/ \alpha^4\left(1 + \mu + \mu\, J_1^2(\alpha)/J_0^2(\alpha)\right) . \qquad (6.5)$$

The smallest root of (6.4) is solved by a Newton-Raphson iteration process, where the initial guess at the root is 2.4048 . This always ensures convergence to the root α , since $0 < \alpha < \alpha_0$, where $\alpha_0 = 2.40482556$ is the smallest root of $J_0(x) = 0$; see Fig. 2 for details. If this is not done, the iteration process will fail to converge to the

correct root because it will predict a root on another branch of the curve $y = J_1(x)/J_o(x)$.

The function $\bar{M}(s)$ in (6.1) is now inverted and compared with the small and large time solutions for different λ , these being the only analytic solutions available.

Typical values of λ are chosen as follows. From (2.9)

$$\lambda = \frac{a^2/D_c}{\ell^2/D_e} ,$$

where ℓ is the thickness of the tissue sample.

For nitrogen, $D_c \sim 2 \times 10^{-10}$ cm^2 sec^{-1} and $D_e \sim 10^{-5}$ cm^2 sec^{-1} . Also $a \sim 15 \times 10^{-4}$ cm ; and .01 cm $\lesssim \ell \lesssim$ 1 cm may be considered a typical set of values for the thickness of a tissue slice. This yields approximately

$$10^{-1} \lesssim \lambda \lesssim 10^3 .$$

Thus we choose $\lambda = 10^{n-2}$, n = 1,2, ..., 5 as a representative set. Naturally the cellular-extracellular diffusion interaction is best demonstrated when $\lambda \sim 1$. It is significant that a typical tissue slice usually chosen for these experiments (about .2 cm) yields a value $\lambda \sim 3$, which is well within the proposed interaction zone of the extra/intra cellular time scales.

Figures 5 and 6 give a set of curves for λ = 1 and 10 showing different numerical inversion compared with the small and large time solutions. It is seen that Piessens method is very accurate for small times but fails rapidly thereafter for both small and large λ . The other methods only behave

peculiarly at very large times, but this is to be expected, since the error is usually proportional to a power of the time. The curves show no essential difference between the Bellman-Kalaba-Lockett method and the Norden method. In fact agreement was usually less than .5% and correct to 3 places. The Norden solution was particularly good, making a smooth transition from the small time solution to the large time solution; agreement was remarkable at very small and very large times, normally to 4 figures. See Table IV. Only a selection of the points are presented, mostly falling on the graphs in figs 5 and 6. The curves were prepared from the full computer output.

It should be noted that in each case some experimentation was performed on the parameters in the numerical inversion method. However computing time becomes very large in an attempt at comprehensive studies of all possible variations, which in any case is outside the scope of the thesis.

No significant improvement was obtained by varying the parameters in the B-K-L and Norden method. However accuracy dropped in the Piessens method when 30 x 30 points and 100 x 100 points were compared with the 50 x 50 points except at small times, where it was excellent. Also a different 'b' was tried in each case, with no significant improvement. Computing time for the 100 x 100 formula was over two minutes per run, which becomes expensive for the results produced. The other runs normally took only half a minute for the set of five values of $\lambda = 10^{n-2}$, $n = 1,2,3,4,5$.

Thus the Norden method of numerical inversion is to be preferred in analysing gas uptake and washout in excised tissue.

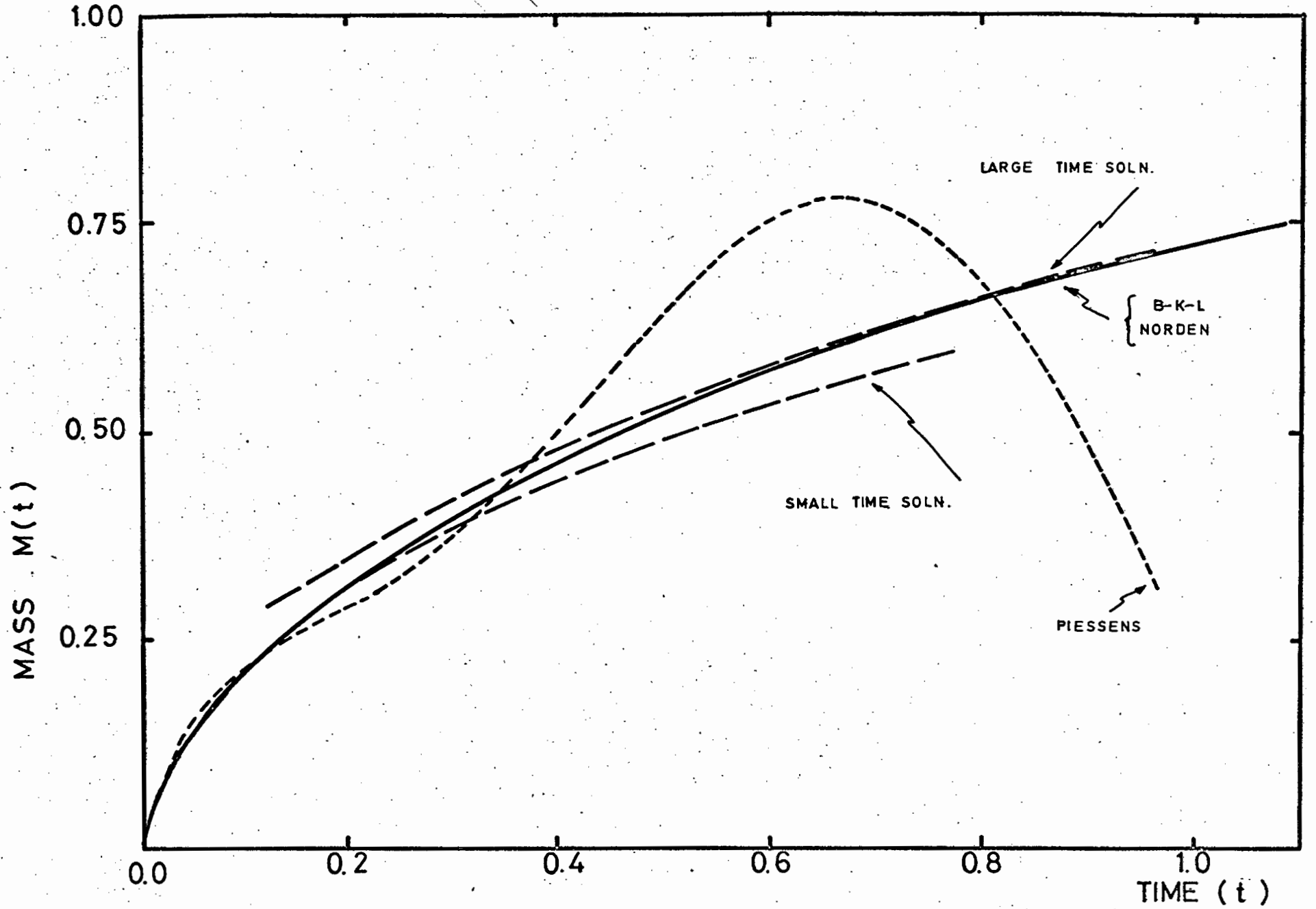

FIG.5 MASS UPTAKE IN EXCISED TISSUE ($\lambda = 1$)

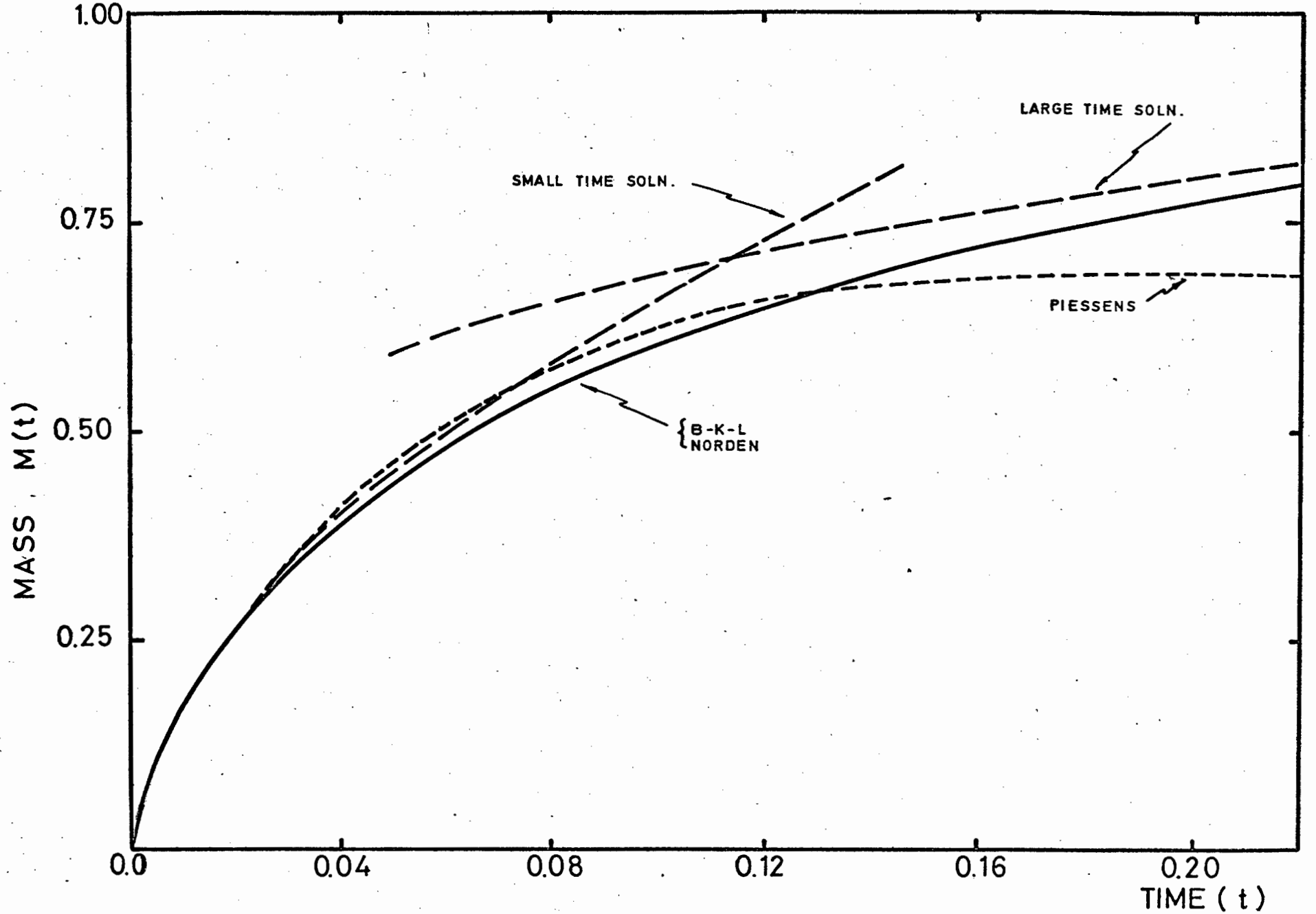

FIG.6 MASS UPTAKE IN EXCISED TISSUE ($\lambda = 10$)

TABLE IV

NUMERICAL INVERSION OF LAPLACE TRANSFORM 6.1

TIME (μ=1.11) (λ=1)	Small Time Solution	NUMERICAL INVERSION			Large Time Solution
		NORDEN 10 pt $x_o=e^{-.6}$ $b=e^{.2}$	B-K-L 10 pt c = o	PIESSENS 50x50 pt a = 1.5 b = 1/8	
.01	.05832	.05832	.05571	.05711	-
.02	.08500	.08506	.08610	.08499	-
.04	.12466	.12502	.12608	.12862	-
.10	.20852	.21051	.20984	.21442	-
.40	.44303	.46402	.46369	.49469	.47818
.80	.60043	.65875	.65894	.67559	.66074
1.50	-	.84002	.84044	-	.84030
2.00	-	.90632	.90638	-	.90677
(λ=10)					
.01	.18443	.18450	.17657	.18085	-
.02	.26870	.26888	.27111	.26857	-
.04	.39420	.39103	.39390	.40172	-
.10	.65938	.60434	.60293	.62109	.68467
.20	.97092	.77376	.77446	.68205	.80199
.30	-	.86225	.86307	.75063	.87566
1.00	-	.99550	.99453	-	.99521
1.50	-	1.00010	.99987	-	.99953

6.3 Numerical Solution for Perfused Tissue

The function to be inverted is given by (3.13)

$$\bar{M}(s) = \frac{\lambda}{s^2(1+\mu)} \left[1-\lambda/(s+2\mu\sqrt{s}I_1(\sqrt{s})/I_o(\sqrt{s})+ \lambda) \right] \qquad (6.6)$$

where λ is now the ratio of cellular diffusion to the blood perfusion time scale.

The small time solution to first order is

$$M_s = \frac{\lambda}{1+\mu}\left(t - \frac{\lambda t^2}{2} + \frac{16\mu\,\lambda\, t^{5/2}}{15\sqrt{\pi}} + \lambda(\lambda-\mu+4\mu^2)\,\frac{t^3}{6}\right) \qquad (6.7)$$

whilst the large time solutio n is taken from the exact solution (3.15) as

$$M_\ell = 1 - Ae^{-\alpha^2 t} \qquad (6.8)$$

where α is the smallest root of

$$\alpha^2 + 2\mu\alpha\, J_1(\alpha)/J_o(\alpha) = \lambda \qquad (6.9)$$

and

$$A = \frac{\lambda^2}{(1+\mu)} \Big/ \alpha^4(1 + \mu + \mu J_1^2(\alpha)/J_o^2(\alpha)) \qquad (6.10)$$

The equations (6.8), (6.9) and (6.10) are analogous to (6.3), (6.4) and (6.5) and a common program is used to generate the results.

We recall that the crucial parameter is

$$\lambda = \frac{a^2/D_c}{1/\mathring{Q}_e}$$

where $\mathring{Q}_e$ is the blood perfusion ml blood/ml tissue/min. Now a^2/D_c is known from the previous section. The blood perfusion is set out in Table V, for some average values of blood flow through human organs. Thus

$$.01 \leq \mathring{Q}_e \leq 5.60 \text{ ml/ml/min.}$$

Hence it is easy to predict that for human tissue,

$$1 \leq \lambda \leq 1000$$

approximately, and thus we choose

$$\lambda = 10^{n-2} \qquad n = 1, 2, \ldots, 5$$

which is conveniently the same range as in the previous section.

TABLE V

PERFUSION IN HUMAN TISSUE

from
Bell, Davidson and Scarborough (1961)

Organ	Perfusion ml/100 gm/min
Thyroid	560
Kidney/Liver	150
Heart	100
Intestine	70
Brain	65
Spleen	40
Stomach	25
Hand	7-12
Finger	15-40
Forearm (muscle)	1-3
Leg (muscle)	1-2

It is significant from Table V that in muscle, $\lambda \sim 1$ where the diffusion-perfusion interaction is maximal. Muscle tissue forms a large proportion of the body and it is clear that if the diffusion and perfusion time scales interact, then neither a perfusion nor a diffusion based theory is adequate to predict the correct uptake behaviour in this tissue type, and the present analysis is thus fully justified.

On the other hand, it is easy to see why the diffusion theory is gaining acceptance in decompression predictions, since the majority of tissues have a $\lambda \gg 1$ where

diffusion completely dominates perfusion. This is commented on more fully in chapter 7.

Figs. 7 and 8 provide comparisons of the numerical inversion of (6.6) with the small and large time solutions (6.7) and (6.8).

Notice that for $\lambda = 1$, the solution rapidly decays to a single exponentially controlled curve (given by (6.8)) as predicted in chapter 3, where a perfusion controlled response can be expected for $\lambda << 1$. In fact the numerical solution for $\lambda = .1$ (not shown for obvious reasons) agrees with the small time and later the large time solution to 7 decimal places, the worst error being about .05%. Thus it is seen that even though (6.6) can be inverted exactly (at considerable effort see (3.15)) it is hardly necessary.

Once again the Piessens solution fails at medium to large times, although it is very good for small times. The computing time and programming effort required seem hardly justified for monotone inverse laplace transforms however. The B-K-L method is generally not quite as accurate as the Norden method although this could be due to a poor choice in parameters.

Table VI contains a selection of points from Figs. 7 and 8 and it is seen that numerical inversion by Norden is in excellent agreement.

Thus it seems possible that experimental data curves can be analysed and compared with the numerical inversion curves with confidence, especially since muscle is a popular tissue

for conducting gas uptake and washout experiments, and $\lambda \sim 1$ in this tissue, where (6.6) is expected to be most effective.

TABLE VI

NUMERICAL INVERSION OF LAPLACE TRANSFORM 6.6

TIME (μ=1.11) (λ=1)	Small Time Solution	NUMERICAL INVERSION			Large Time Solution
		NORDEN 10 pt $x_o = e^{-.6}$ $b = e^{.2}$	B-K-L 10 pt c = o	PIESSENS 50x50 pt a = 2 b = 1/8	
.01	.00472	.00472	.00447	.00472	-
.02	.00940	.00940	.00994	.00940	-
.04	.01870	.01866	.01915	.01866	.01971
.10	.04641	.04573	.04508	.04572	.04633
.40	.20805	.16896	.16804	.16902	.16900
.80	-	.30837	.30922	.30734	.30836
1.50	-	.49842	.50068	.50603	.49840
2.00	-	.60124	.59658	.57397	.60125
(λ=10)					
.01	.04545	.04536	.04532	.04547	-
.02	.08797	.08723	.08724	.08738	-
.04	.16878	.16250	.16251	.16223	-
.10	.44623	.33999	.33400	.33738	.37928
.20	-	.53920	.53923	.54637	.55043
.30	-	.67129	.67121	.69454	.67439
1.00	-	.96607	.96595	-	.96596
1.50	-	.99461	.99322	-	.99322

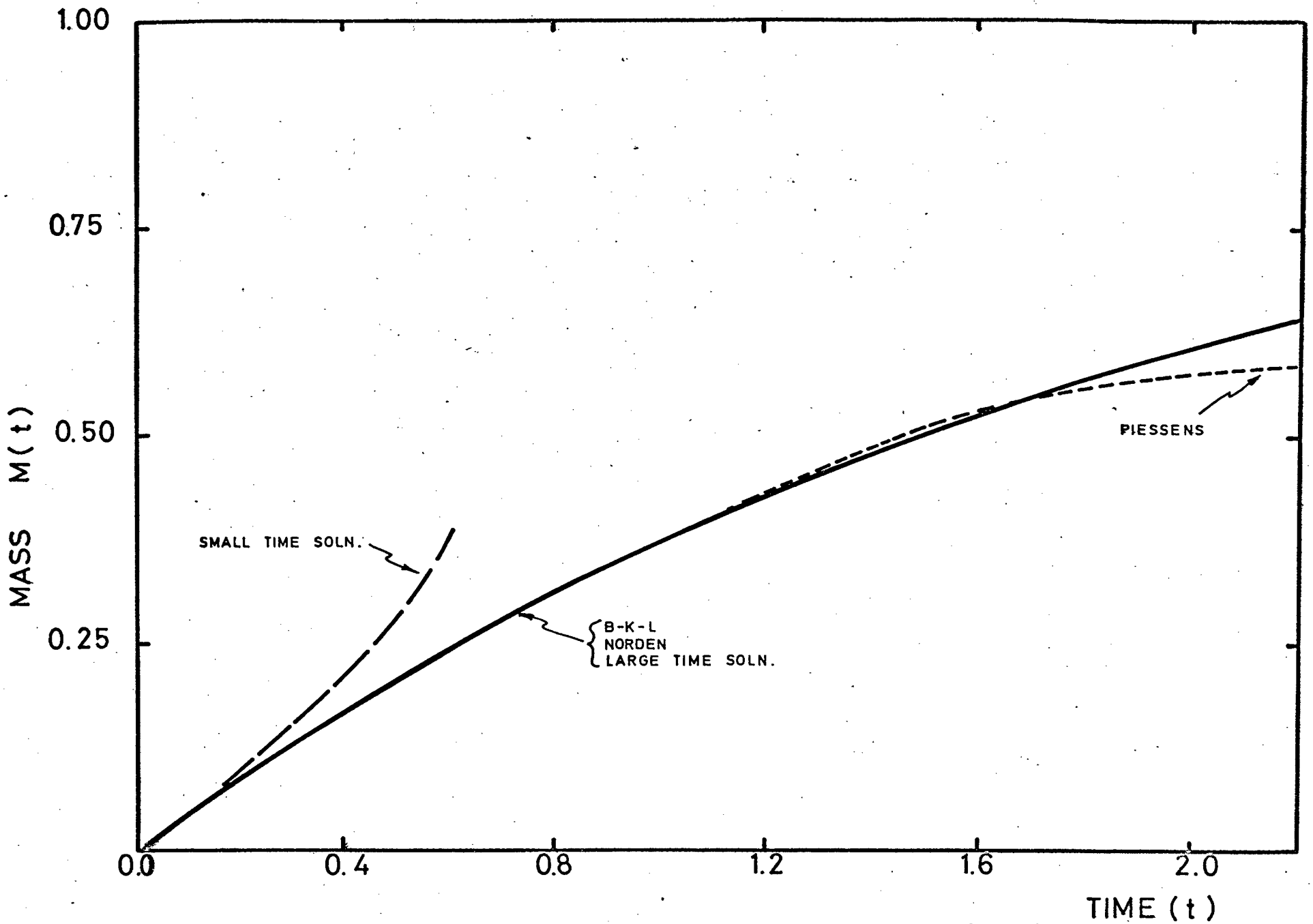

FIG. 7 MASS UPTAKE IN PERFUSED TISSUE ($\lambda = 1$)

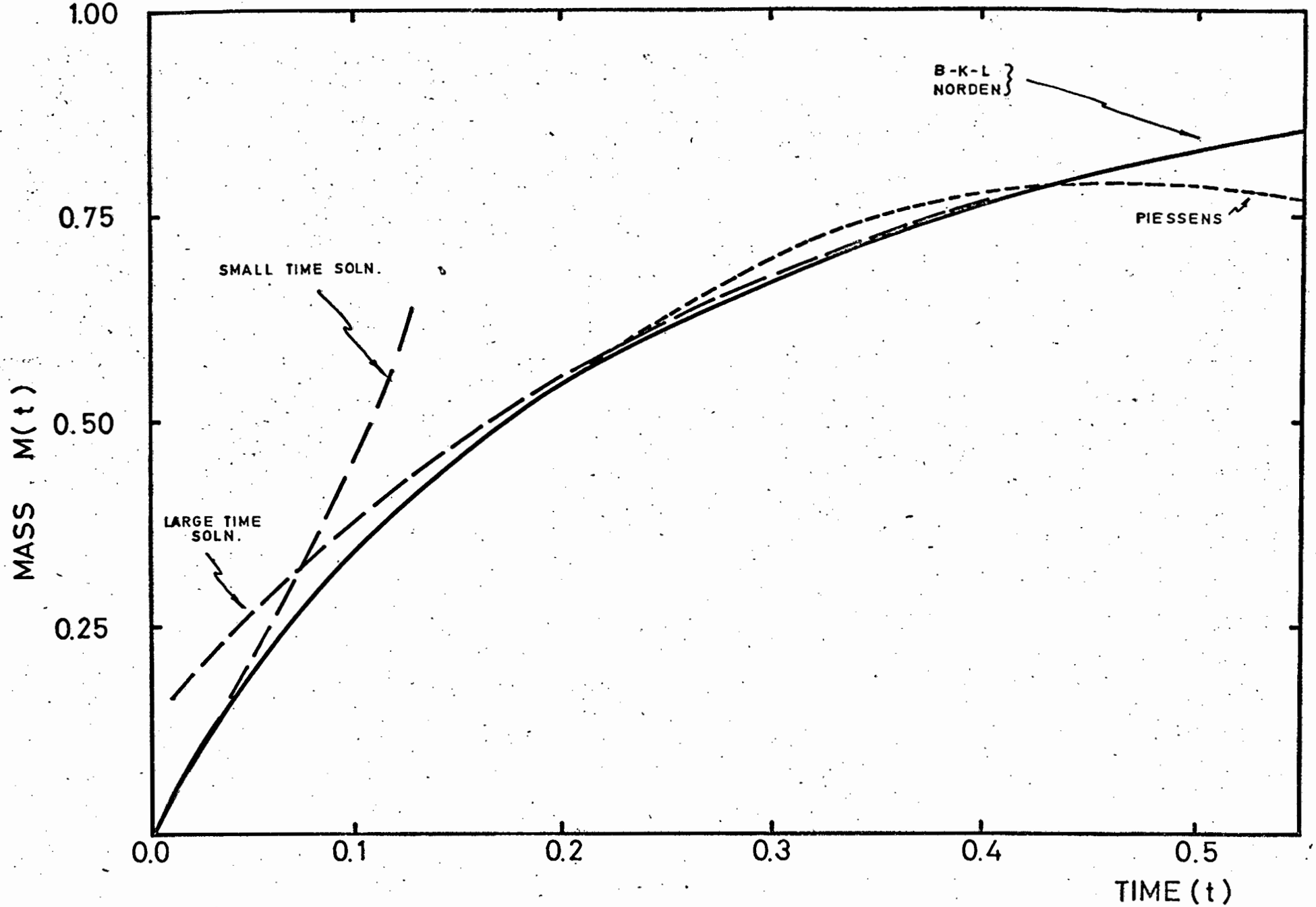

FIG.8 MASS UPTAKE IN PERFUSED TISSUE (λ=10)

6.4 Numerical Inversion of the axially dependent model

We wish to invert the function from (5.14) and (5.16):

$$\bar{p}(s) = \frac{\lambda}{s^2(1+\mu)} \left(1 - \exp\left\{ - \frac{s}{\lambda} + \frac{2S_p\sqrt{s}}{\lambda\alpha} \frac{f(\alpha,s)}{g(\alpha,s)} \right\}\right) \quad (6.11)$$

where
$$\left.\begin{aligned} f(\alpha,s) &= I_1(\alpha\sqrt{s})\, K_1(\sqrt{s}) - I_1(\sqrt{s})\, K_1(\alpha\sqrt{s}) \\ g(\alpha,s) &= I_o(\alpha\sqrt{s})\, K_1(\sqrt{s}) + I_1(\sqrt{s})\, K_o(\alpha\sqrt{s}) \end{aligned}\right\} \quad (6.12)$$

The method chosen was that of Norden, and it was decided that further comparison with others was unnecessary, owing to the excellent results obtained with Norden's method. Instead of simply computing the uptake curves of sections 6.2 and 6.3 (which were useful from a point of view of comparison with likely experimental uptake curves), we compute the half-time of the tissue and plot this against the perfusion P, as being the best method of illustrating the perfusion diffusion interaction.

The half-time is that time at which the tissue is 50% saturated from its initial to its final tension. In dimensionless units, this simply requires $p(t) = .5$, since the initial tension is zero, and final tension unity.

The method of converging to the half-time was considered from several points of view. The final choice was the method of successive bisection. Even though slow, it is extremely stable in our case (since there is only one root $p = .5$ in the range $0 < t < \infty$) and once one half-time has been found for a given P, all others follow easily, since there will exist a good guess from the previously found half-time. The algorithm required a little modification since whilst a lower

limit to the root always exists ($t = 0$) there is no finite upper limit. Thus each search commenced with a quick check by successive halving or doubling to produce an upper limit to begin the main algorithm. Five figure accuracy was sought, and so iterating was terminated after 30 steps and an error message printed. However this never occurred in the numerical experiments.

For each run we select a value for

(i) the partition coefficient S_p, 1.0 for aqueous, 5.0 for lipid tissue,

(ii) the basic diffusion time scale a^2/D_c, 7.752 minutes (Hills, 1966), 9.456 minutes (chapter 2, based on $\alpha = {}^1/5$) and two purely aqueous values of 10^{-3}, 10^{-4} minutes for comparison.

(iii) the vascularity $\alpha(= a/b)$ ${}^1/5$, ${}^1/10$, ${}^1/15$ and ${}^1/20$; the last two were considered a little unrealistic in the sense that the average cell is about 30μ in diameter, and the radius of capillary about 4-5μ giving an $\alpha \sim {}^1/10$ as a likely lower limit.

(iv) typical values of the perfusion P, measured in ml blood per ml tissue per minute were taken from Table 5, where we have $.01 \lesssim P \lesssim 5.6$ ml/ml/min. Thus P was chosen $10^{-4} \lesssim P \lesssim 10$ on the basis that it seems possible that very low perfusion rates may occur in cases of partial vasoconstriction, or simply in zones of low vascularity in resting tissue. But it should be recalled that $P \sim 10^{-2}$ is a common value for muscle tissue.

The actual diffusion time scale/perfusion time scale ratio λ is calculated from the formula $\lambda = a^2/d_c \; P/\alpha^4$, using 5.20.

The dimensionless half-time is converted to minutes by

multiplying it by the factor $\frac{a^2/D_c}{\alpha^2}$, where it will be recalled that the dimensionless time was defined by t', $t = b^2/D_c\, t'$.

When P is large, λ is large, and so there is clearly a loss of precision in evaluating (6.11). Accordingly, the exponential is expanded in a power series for large λ ($\lambda \gtrsim 10^3$ was chosen), which allows $\bar{p}(s)$ to be evaluated to its original high precision.

On the same graph we wish to plot the curve for the perfusion or Haldane half-time given by (5.21):

$$T = (\alpha^2 + (1 - \alpha^2)S_p)\log 2/P \text{ minutes}, \qquad (6.13)$$

and the diffusion half-time, got by solving the half-time from (5.22) and (5.23) for each α and a^2/D_c . However this was not done in the latter case directly because the numerical inversion converged to this value in an unmistakable manner. This half-time will be called the Hills half-time even though it is not strictly so (see the note after equation (5.23)). To illustrate these three curves, a log-log plot is chosen. In this case the Haldane half-time becomes a straight line inclined at -45° , and is unvarying for different α , if $S_p = 1$, an added advantage for comparison. The Hills half-time is independent of the perfusion and is thus a horizontal line. The numerical inversion is shown plotted in figures 9 , 10 for various vascularities.

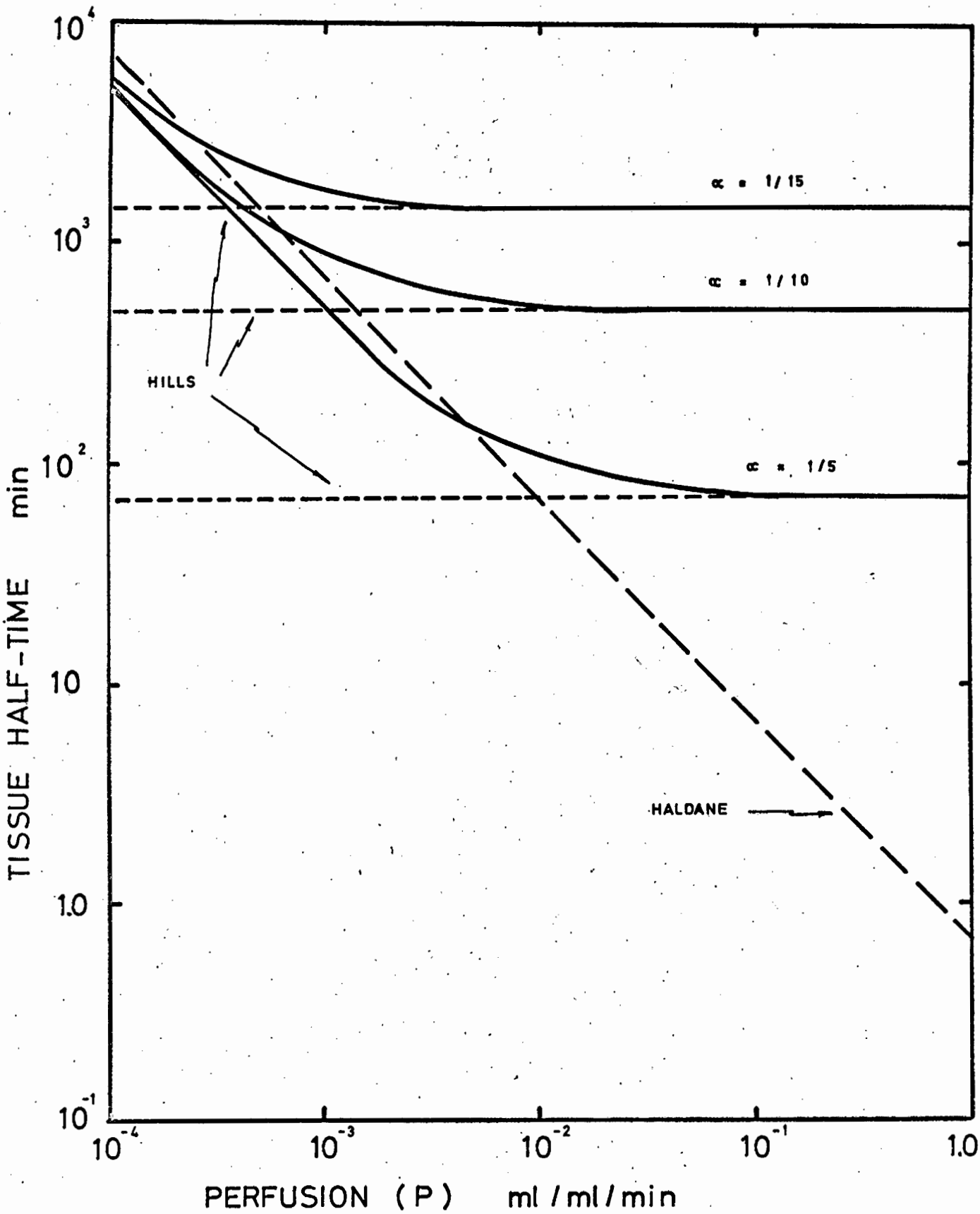

FIG. 9. HALF-TIME CURVES IN A HOMOGENEOUS CELLULAR TISSUE.

($S_p = 1$, $a^2/D_c = 9.456$ min)

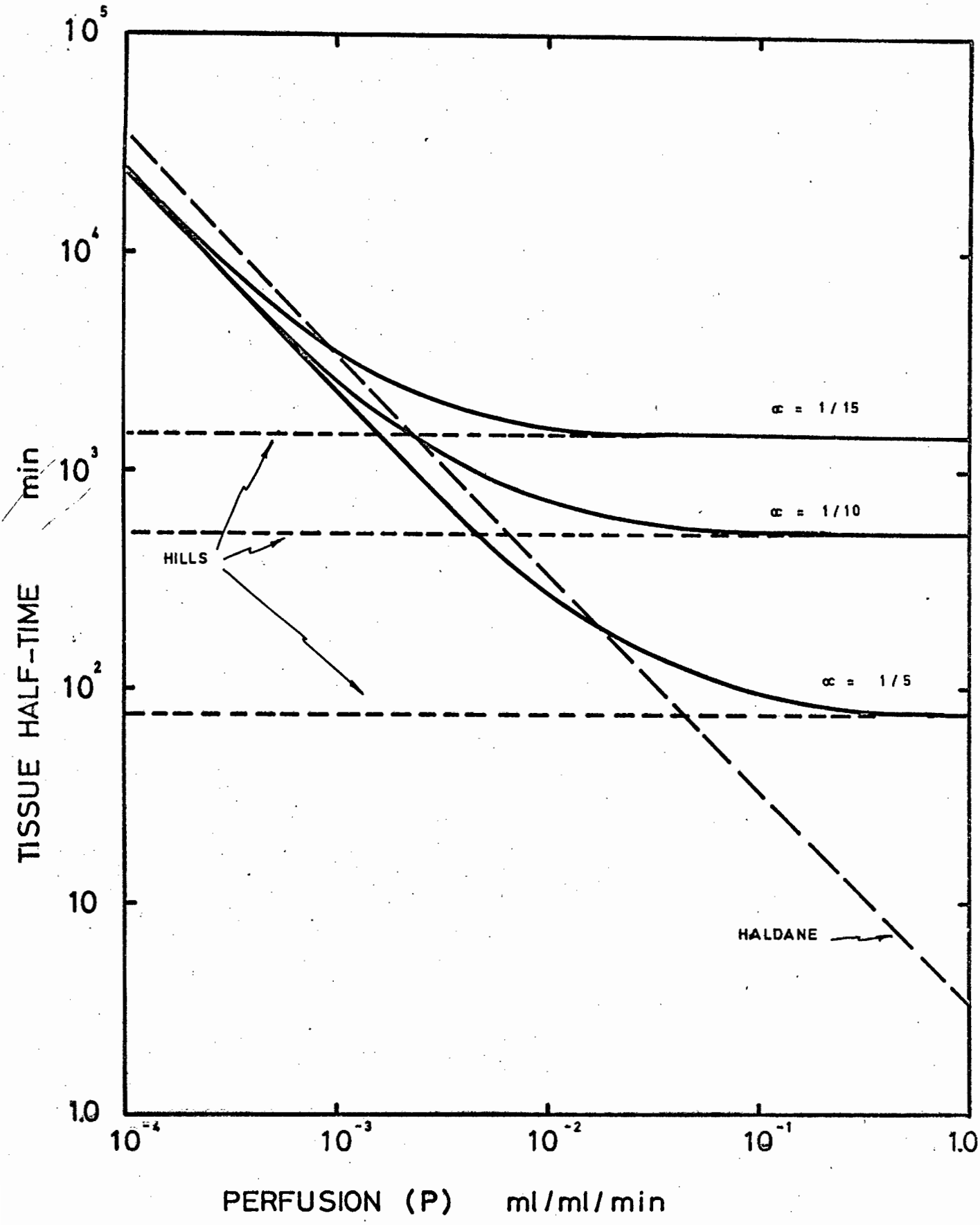

FIG. 10. HALF-TIME CURVES IN A HOMOGENEOUS CELLULAR TISSUE.

(S_p = 5 , a^2/D_c = 9.456 min)

A copy of the program will be found in Appendix A.

Tables 7 and 8 show some typical values for an aqueous type tissue ($S_p \sim 1$) and a lipid type tissue $S_p \sim 5$. All the half-times are longer, of course, and there seems to be a general shift towards a diffusion based system.

TABLE SEVEN

AQUEOUS TISSUE HALF-TIMES OVER A PERFUSION SPECTRUM

($S_p = 1.0$, $a^2/D_c = 9.456$ min)

Hills value is the limit of cols 2, 3, 4.

PERFUSION ml/ml/min	TISSUE HALF-TIMES (MINUTES)			
	$\alpha = 1/5$	$\alpha = 1/10$	$\alpha = 1/15$	HALDANE
0.0001	4947	5071	5683	6932
0.001	518	887	1788	693
0.01	108	534	1456	69
0.1	73	502	1424	7
1.0	69	499	1421	.7
10.0	69	498	1421	.07

It will be noticed that for a given perfusion and vascularity, significant differences always exist between the actual and the Haldane half-time, except where the curves cross. On the other hand, the actual half-time merges smoothly with the Hills half-time for large perfusion rates but diverges for small P . The most significant finding is that in the region P ~ .01 (muscle tissue) and $\alpha \sim 1/5$, there is a

zone where

(i) all three half-times are a similar order of magnitude

(ii) the actual half-time is longer than the others.

In other words (i) implies that on a casual analysis it will be very difficult to decide whether perfusion or diffusion is dominant in regions where $P \sim .01$ and (ii) implies that in actual fact there is an interaction between perfusion and diffusion to create a longer half-time.

For smaller values of the vascularity, the effect begins to disappear and diffusion dominates as to be expected. On the other hand it can be seen that even for large values of the perfusion, diffusion still controls the uptake half-time. This may at first seem surprising, however it should be realised that those organs which have a large perfusion require this for metabolic reasons, and this effect has been ignored in this thesis. Thus whilst increasing the perfusion by a large amount will not increase the half-time of the tissue for an inert gas, it will of course replenish depleted oxygen tension on high metabolic demand.

Two runs were tried using very low values of the diffusion time scale (.001 , .0001 min), and it is confirmed that the actual curve closely follows Haldane's curve as to be expected since this is the basis of the perfusion theory.

It will be noticed that for very low values of the perfusion the Haldane curve and actual curve are parallel. It is of interest to calculate this difference theoretically and compare with the numerical output.

TABLE EIGHT

LIPID TISSUE HALF-TIMES OVER A PERFUSION SPECTRUM

($S_p = 5$, $a^2/D_c = 9.456$ min)

PERFUSION ml/ml/min	TISSUE HALF-TIMES (MINUTES)			
	$\alpha = 1/5$	$\alpha = 1/10$	$\alpha = 1/15$	HALDANE
.0001	23956	24541	24832	33549
.001	2397	2671	3439	3355
.01	279	690	1608	335
.1	91	522	1446	34
1.0	74	506	1430	3
10.0	73	505	1429	.3

As $P \to 0$, $\lambda \to 0$ and (6.11) degenerates to

$$\bar{p}(s) \sim \frac{\lambda}{1+\mu} \frac{1}{s^2}$$

Thus as $P \to 0$,

$$p(t) \to \frac{\lambda}{1+\mu} t ,$$

constant rate of increase, as to be expected in cases where V is very low. On the basis, of this equation, the actual half-time for very low values of the perfusion approaches

$$T_H = 2(1+\mu)/2\lambda$$

which in dimensional units, and $S_p = 1$, is

$$T_H = 1/2 P .$$

The log of this term is to be subtracted from the log of the Haldane half-time given by (6.13) and the result is obviously

$$\log_{10} \log_e 4 = .1419 ,$$

which is in satisfactory agreement with the numerical inversion result of .1461. (The error is acceptable in that the half-time is very large, where the numerical method starts to yield poor results).

Thus to conclude this section, it is seen that the Haldane solution is at best an asymptotically orientated technique which gives too high a half-time over a wide range of small perfusion, and too small a half-time for large P. It is only marginally correct in the interaction zone. On the other hand the Hills type diffusion approach is accurate for large perfusion rates but very poor for small perfusion zones. In general it is to be preferred to the Haldane approach.

At first sight, our model may appear to be too complicated to be of practical use (the Hills model likewise).

However the program used to generate the solutions on a modern computer with adequate library software is quite short. It can thus be seen why the Haldane theory persisted for so many years. It is conceptually straightforward and computationally simple. If it fails to provide a good fit, simply 'adjust' the half-time until the data curve gives a reasonable fit. Thus for example, Haldane employed 5 tissue half-times for his early decompression tables. Over the intervening years more and more half-times had to be invented to fit the facts. Today the U.S. Navy employ up to 14 half-times to provide Oxy-Helium decompression table predictions

based on the Haldane Perfusion theory. Clearly with so many parameters virtually any theory can be made to fit a data curve. Hills (1966) diffusion theory on the other hand requires only two parameters (the vascularity and diffusion time scale) to give a convincing analysis of decompression schedules for exposures to a pressure equivalent to 60m sea depth.

It is suspected that to carry the validity of decompression calculations to greater depths, the third parameter, the perfusion, must be included as shown in this chapter.

6.5 Other Numerical Approaches

Throughout this thesis, all transport equations have been solved by the Laplace Transform. However, the only reason why this method was preferred is simply that it provides the solution of relevant equations, after various terms have been ignored on carefully justified grounds.

If on the other hand these terms may not be ignored, then the Laplace transform method becomes unwieldly indeed. In these cases we would have to sacrifice insight into the problem by being unable to obtain the small and large time analytical solutions provided by the Laplace transform method.

The next step is an attempt on finite difference methods of solution, for example alternating direction implicit methods. However the mere setting up of the finite difference equation for the model of chapter five is a formidable task in itself. The problem is two-dimensional in space coordinates and has derivative boundary conditions on all four boundaries! This can be seen by inspecting the appropriate

set of equations below (taken from (5.9), (5.10) and (5.13):

$$\frac{\partial u}{\partial t} = \frac{1}{r}\frac{\partial}{\partial r}\left(r\frac{\partial u}{\partial r}\right) + \beta\frac{\partial^2 u}{\partial z^2} \quad ,$$

$$0 < \alpha \lesssim r \lesssim 1 \ , \quad 0 \lesssim z \lesssim 1 \ , \quad t > 0 \ ,$$

subject to the following boundary conditions:

(i) $\dfrac{\partial u}{\partial t} = -\lambda\dfrac{\partial u}{\partial z} + \dfrac{2S_p}{\alpha}\dfrac{\partial u}{\partial r}$,

$$r = \alpha \ , \quad 0 \lesssim z \lesssim 1 \ , \quad t > 0 \ .$$

(ii) $\dfrac{\partial u}{\partial r} = 0 \ , \quad r = 1 \ , \quad 0 \lesssim z \lesssim 1 \ , \quad t \gtrsim 0 \ .$

(iii) $\dfrac{\partial u}{\partial z} = 0 \ , \quad z = 0 \ , \quad \alpha \lesssim r \lesssim 1 \ , \quad t \gtrsim 0 \ .$

(iv) $\dfrac{\partial u}{\partial z} = 0 \ , \quad z = 1 \ , \quad \alpha \lesssim r \lesssim 1 \ , \quad t \gtrsim 0 \ .$

(v) $u = 1 \ , \quad r = \alpha \ , \quad z = 0 \ , \quad t > 0 \ .$

and finally the initial condition $u = 0 \ , \ t = 0 \ ,$

$$\alpha \lesssim r \lesssim 1 \ , \quad 0 \lesssim z \lesssim 1 \ .$$

Unfortunately even at the present time ADI methods with derivative boundary conditions have not been developed to the state where the above problem could be solved with confidence.

In fact a separate project in itself would be the comparison of the Laplace transform solution with an A.D.I. solution in the case $\beta = 0$.

CHAPTER 7

CONCLUSION

In this final chapter, we attempt to link up the various models via their characteristic time-scales T_C , the cellular time-scale, the interstitial time-scale T_I and the perfusion time-scale T_P .

As was sketched briefly in Chapter 1, all these scales can be made to assume a wide spectrum of inter-relationships with each other. Auto-regulation and vaso-motion control the rate of oxygen input to the tissue zone, and thus blood perfusion alters, thereby changing T_P . However for a given tissue state (that is a specific metabolic demand) there will be a specific blood perfusion and thus T_P may be defined for that tissue as the average over some appropriate time. Also a typical vascularity may be defined as a result, and thus T_I and T_C become fixed for that state.

It is not certain how the vascularity of the tissue responds to short period changes in metabolic demand. Over long periods of hypoxia, the vascularity does in fact increase in a permanent way. It also appears to increase slightly on sudden muscular effort by the widening of capillaries from about 8 to 10 m . Naturally in the latter case, the blood-flow increases and capillaries now have a higher <u>average</u> blood velocity. Yet this does not necessarily mean that some capillaries which were closed before the exercise now open up. Rather that the frequency of opening is increased, as is the period of remaining open. In other words it is conjectured that the vascularity may be constant for a given tissue over a

range of exercise levels. This appears to be born out in the correlation of decompression formats by Hills (1966), who discusses three exercise levels with the reciprocal of the vascularity as 4.73, 4.91, 5.29, varying from rest to heavy work. The vascularity change here is small (but significant). Now the interstitial fluid is mainly aqueous and can only have a large time-scale if the vascularity is very low, (almost avascular). This is not the case in most tissues of the body.

Thus it is possible that the interstitial time-scale - T_I is a fairly low constant in normal conditions. The cell diameter is also uniform and so T_C may be supposed constant for a given tissue.

It appears from the foregoing that a given tissue zone may have a variable T_P, a low T_I and a constant T_C over quite a wide range of exercise levels. For muscle $T_P \sim T_C$, as seen in Figure 9 (we can identify the half-time as the time-scale here). In excised tissue $T_P \sim \infty$, a special case and one is then concerned with the relative magnitudes of T_I and T_C.

Contrast the above remarks on the likely time-scales in tissue to that of Table IX, where an exhaustive list of realistic combinations of T_C, T_I and T_P are presented. All cases except four have been the subject of a mathematical model at some time. We have listed for clarity Haldane as representative of the perfusion approach, Hempleman the aqueous diffusion approach, Hills the cellular diffusion and perfusion/diffusion interaction approach, along with the approaches of chapter 2, 3 and 5.

TABLE IX

COMPARISON OF PERFUSION-DIFFUSION MODELS

MAIN APPROACH		SECONDARY APPROACH	REMARKS
MAINLY PERFUSION	1	$T_I \ll T_P$	Haldane (1908) similar to 4.
THEORY	2	$T_I \sim T_P$	low vascular acellular tissue solve using No. 5.
$T_C \sim 0$	3	$T_I \gg T_P$	Hempleman (1969) similar to 7.
PERFUSION AND	4	$T_C \ll T_P$	Chap 5 (axial dep) Haldane (1908) see 4.
DIFFUSION	5	$T_C \sim T_P$	Chap 5 (axial dep) Chap 3. Hills (1967).
$T_I \sim 0$	6	$T_C \gg T_P$	Chap 5 (axial dep) Hills(1966) see 6.
DIFFUSION	7	$T_C \ll T_I$	Hempleman (1969) see 3.
THEORY	8	$T_C \sim T_I$	high vascular low cellular tissue, solve using No. 11.
$T_P \sim 0$	9	$T_C \gg T_I$	Hills (1966) similar to 6.
EXCISED TISSUE	10	$T_C \ll T_I$	Krogh (1919)
	11	$T_C \sim T_I$	Chap. 2. Hills (1967)
$T_P \sim \infty$	12	$T_C \gg T_I$	unlikely, very thin tissue slice: damage to cells.

Note (i) $T_C \sim \infty$, $T_I \sim \infty$ considered unlikely.

(ii) $T_C \sim T_I \sim T_P$ unknown tissue type.

The diffusion model arising from chapter 4 (D a linear function of pressure) is considered unlikely, except for the fact that the diffusion time-scale is of the correct order of magnitude. This is the main result of chapter 4.

It has been shown in chapter 6 that in the perfused case, No. 5 and 6 appear to be the most important approaches and No. 11 in excised tissue.

It was also shown in section 6.3 that the great majority of tissues exhibited a $\lambda(= T_C/T_P) >> 1$, except for muscle tissue where in section 6.4, a strong interaction appeared ($T_C \sim T_P$) . This seems to be contradictory in the sense that the main variable is T_P and yet for most tissues $T_P << T_C$. However as was noted in section 6.4, the point is that we have been discussing the uptake of an inert gas in the tissue. In the case of oxygen, it is not necessarily so that $T_P << T_C$, if the oxygen is continually consumed in the cell.

In other words, it seems reasonable to conclude that cellular diffusion is the main factor controlling gas uptake in tissue, but that in muscle tissue an interaction with perfusion occurs.

The other cases shown do not appear to have been singled out for analysis before, but can be solved by means of the models proposed in the thesis.

A special case not discussed is that where $T_C \sim T_I \sim T_P$. The reason for this is mainly one of identifying a tissue structure where this feature is predominant. In any case the mathematical model would be an order of magnitude more complex than the present models.

APPENDIX A

NUMERICAL INVERSION OF THE LAPLACE TRANSFORM

Because many of the formulae derived in the present work require inversion, it was decided to investigate an appropriate method of numerical inversion of the Laplace transform. An extensive literature survey was undertaken which uncovered a surprisingly large and interesting range of methods. It may be useful to attempt a brief summary of the main approaches. An up to date review is given by Luke (1969).

There appear to be four main criteria guiding a choice of quadrature inversion formula

(i) the Laplace transform is not known analytically (for example as the solution to a differential equation). This means a quadrature formula must be selected at real, usually equidistant points on the s plane.

(ii) the Laplace transform is known as a reasonably simple analytical function. Here it is likely that a quadrature formula can be selected which uses complex equi or non-equi-distant points on the s plane according to taste.

(iii) the Laplace transform is a known but very complex analytical function. In this case it may be totally unsuitable to use complex values on the s plane (consider for example the computation of $K_n(\sqrt{x+iy})$. Thus a real quadrature formula would be used.

(iv) irrespective of whether the Laplace transform is known analytically or not, it must be decided at the outset the form of the time values desired, namely equal interval, unequal interval (a geometric progression for example) or continuous.

(iv)(continued)

Each has its own advantages. Some of the non-continuous (in time) quadrature formulae can be fixed up to provide continuous data by suitably adjusting various parameters.

It should be noted that we are not concerned here with the actual amount of computing time required for a method to yield a certain accuracy. Thus Atkinson and Lang (1972) examine four methods purely from the number of function evaluations needed to invert the Laplace Transform. Our approach would be more along the lines of high accuracy 'at any price'.

We define the Laplace Transform as

$$F(s) = \int_0^\infty e^{-st} f(t)dt \qquad (A.1)$$

clearly the Laplace inversion of the function $F(s)$ always satisfies

(a) $f(t) \to 0$ as $t \to 0^+$ (zero saturation initially)
(b) $f(t)$ is continuous $t \in [0 , \infty)$
(c) $f(t) \to 1$ as $t \to \infty$ (saturation) ,

and hence $F(s)$ always exists. (Churchill, 1958)
The complex inversion formula is

$$f(t) = \frac{1}{2\pi i} \int_{c-i\infty}^{c+i\infty} e^{st} F(s)ds \qquad (A.2)$$

where c lies to the right of all the singularities of $F(s)$ on the s plane.

On examining the functions (6.1), (6.6) and (6.11) , it is seen that evaluating the Laplace transform at complex points on the s plane is not realistic. This then

eliminates the methods of Dubner and Abate (1968), Piessens (1969), Zakian (1969), Krylov and Skoblya (1969) and Stehfest (1970), which although continuous in time, all employ complex function evaluations.

The remaining methods can be divided into three groups:

(i) that of Erdelyi (1943), Lanczos (1956), Miller and Guy (1966), Bellman, Kalaba and Lockett (1966), Luke (1969), Piessens (1969 b), which all involve replacing (A.1) by a quadrature formula (that is treating (A.1) as an integral equation);

(ii) that of Salzer (1958), Shirtliffe and Stephenson (1961), Norden (1961) and Piessens (1972) which involve replacing (A.2) by a quadrature formula;

(iii) Luke (1969) and Longman (1972) which replace F(s) by a rational approximation (usually a Padé approximation).

From the methods of group (i) we choose the Bellman-Kalaba-Lockett (BKL) method because it has been used quite satisfactorily on functions exhibiting the main features of f(t) above. A similar decision guided the selection of Norden's method which was originally developed to solve some problems in heat conduction in cylindrical systems, Norden (1962), Norden and Seppa (1964). Recently Hanson-Mild (1972) presented a variation on the method which converts it to a continuous time inversion formula, where good results were obtained.

Finally, the Piessens method was selected because of ultra-high accuracy claimed, in a comparison between Salzer's and Luke's methods. A rational approximation method was not tried owing to the complexity of the functions to be inverted.

We now give brief descriptions of the methods.

I The B-K-L Method

Put $t = -\frac{1}{b}\log\lambda$ in (A.1), and define

$$f(t) = b\, e^{ct}\, g(bt) .$$

The result follows easily:

$$F(bs + c) = \int_0^1 \lambda^{s-1}\, g(-\log\lambda)d\lambda .$$

Replace the integral by the N point Gause-Legendre quadrature formula:

$$F(bs_j+c) \simeq \sum_{i=1}^{N} w_i\, \lambda_i^{s_j-1}\, g(-\log\lambda_i) + E_N \qquad (A.3)$$

$$j = 1 , 2 , \ldots , N.$$

where s_j are a suitable set of points, λ_i are the roots of the shifted Legendre Polynomials

$$P_N^*(x) \quad (= P_n(1 - 2x))$$

and w_i the weights $= \int_0^1 \frac{P_N^*\, dx}{(x-x_i)P_N^{*1}(x_i)}$

E_N is the associated error (see Luke (1969), B-K-L (1966) omits this).

It is now required to invert (A.3) to solve for g and thence $f(t)$. Not surprisingly the matrix $w_i\, \lambda_i^{s_j-1}$ is ill-conditioned, reflecting the unboundedness of the Laplace Transform. Thus we must choose the set of points s_j in order that (A.3) may be inverted with a high precision, preferably as an explicit inverse.

It is shown that by choosing $E_N = 0$ and

$s_i = i$, $i = 1$, 2 , ... N , then (A.3) can be solved as desired.

The result is then

$$f(- \frac{1}{b} \log \lambda_i) = b \lambda_i^{-c/b} \sum_{j=1}^{N} A_{ij} F(jb + c) \qquad (A.4)$$

where A_{ij} is the explicit inverse of $w_i \lambda_i^{s_j - 1}$.

Unfortunately $- \frac{1}{b} \log \lambda_i$ is an inconvenient point of time (this is the main drawback in the B-K-L m ethod). Thus a continuously variable value of b is selected so that

$$t = - \log \lambda_i / b \quad ,$$

and λ_i is chosen in the nearest appropriate range of values. A separate subprogram selects i and b given t . The parameter c is open to experimentation. For example if $f(t)$ displays a marked exponential behaviour for large t , c would be chosen accordingly, with the likelihood of (A.3) being a better approximation. Notice too that with b and s already selected, the choice of c controls to some extent the range over which $F(bs_j + c)$ is to be evaluated.

Thus

$$f(t) = b_i e^{-ct} \sum_{j=1}^{N} A_{ij} F(jb_i + c) \qquad (A.5)$$

where $b_i = - \log \lambda_i / t$.

The roots of λ_i of $P_N^*(\lambda_i)$ and w_i are taken from B-K-L (1966) and read in as data.

The method of obtaining the explicit inverse A_{ij} is

straightforward using lagrange multipliers and is given by B-K-L (p 35), with the result:

$$A_{ij} = \underset{x^i}{\text{Coeff}} \left(\frac{P_N^*(x)}{(x-x_j)P_N^{*\prime}(x_j)} \right) . \qquad (A.6)$$

where $P_N^*(x_j) = 0$.

The coefficients of the polynomial $\frac{P_N^*(x)}{x - x_j} \left(= \sum_{k=o}^{N-1} b_{jk} x^k \right)$

is found by using a standard synthetic division algorithm, and using the fact that

$$P_N^*(x) = \sum_{r=o}^{N} \frac{(-1)^r (N+r)! x^r}{(r!)^2 (N-r)!}$$

The coefficients in $P_N^*(x)$ are all integers, which grow very large for large N , which results in accuracy loss. Finally

$P_N^{*1}(x_j)$ is evaluated by using the well-known recurrence relation for Legendre polynomials adapted for use with the shifted legendre polynomial P_N^* .

In practice, $N \sim 10$ is considered a satisfactory order (the largest coefficient in $P_N^*(x)$ is 2,333,760) whereas for $N = 15$, it is $\sim 10^{10}$) .

II THE NORDEN METHOD

The following derivation is similar to that of Norden (1961).

We have

$$L^{-1}(F(s)) = f(t) = \frac{1}{2\pi i} \int_{c-i\infty}^{c+i\infty} e^{st} F(s) ds \quad ;$$

put $s = s'/t$ and drop primes:

$$t\, f(t) = \frac{1}{2\pi i} \int_{\varepsilon-i\infty}^{\varepsilon+i\infty} e^{s} F(s/t)\, ds \ .$$

Replace the integral by an N-point quadrature formula:

$$t\, f(t) = \sum_{i=1}^{N} H_i(t)\, F(s_i/t) + E_N \qquad (A.7)$$

for some H_i , s_i . We require that the formula be exact ($E_N = 0$) when $f(t)$ is expressible as

$$t\, f(t) = \sum_{k=1}^{N} a_k\, t^{k/2} \ .$$

This is the same as requiring that $F(s)$ should be well approximated by $\sum_{k=1}^{N} b_k/s^{k/2}$ which is similar to the Salzer (1958) approach. This approximation conforms to the functions in chapter six when s is small (t large) .

Now

$$L(f(t)) = F(s) = \sum_{k=1}^{N} a_k \frac{\Gamma(k/2)}{s^{k/2}}$$

Thus

$$f(t) = \sum_{k=1}^{N} a_k\, t^{k/2-1} = \frac{1}{t} \sum_{i=1}^{N} H_i(t) \sum_{k=1}^{N} a_k \frac{\Gamma(k/2)}{s_i^{k/2}}\, t^{k/2}$$

$$= \sum_{k=1}^{N} a_k\, t^{k/2-1} \left(\sum_{i=1}^{N} H_i(t) \frac{\Gamma(k/2)}{s_i^{k/2}} \right)$$

$$\text{Thus} \quad \sum_{i=1}^{N} H_i/s_i^{k/2} = 1/\Gamma(k/2) \qquad (A.8)$$

and H_i thus are independent of t .

Choose $s_i = x_o b^i$, $i = 1, 2, \ldots N$, for some suitable x_o , b .

Thus (A.8) becomes!

$$\sum_{i=1}^{N} H_i \, b^{-ik/2} = x_o^{k/2}/\Gamma(k/2) \ , \qquad (A.9)$$

and (A.7) gives:

$$f(t) = \frac{1}{t} \sum_{i=1}^{N} H_i \, F(x_o b^i/t) \qquad (A.10)$$

In practice b is chosen near 1^+ , and $x_o < 1$.

Equation (A.9) is inverted by a double precision matrix inversion package. The gamma functions are easily calculated by a factorial relation since k is integral.

In the original method, a formula using a geometric progression of points in time was used instead of (A.10). (This innovation is due to Dr.K. Hansson-Mild and the writer is grateful to him for a copy of his program, where this was first noticed).

III THE PIESSENS METHOD

We expand $F(s)$ in a series of Jacobi Polynomials $P_k^{(\alpha,\beta)}$:

$$F(s) = s^{-a} \sum_{k=o}^{\infty} c_k \, P_k^{(\alpha,\beta)}(1 - {}^{b}/_{s}) \ , \qquad (A.11)$$

valid for $b/2 \leq s \leq \infty$,

where α , β, a and b are free parameters, and

$$c_k = \frac{1}{h_k} \int_{-1}^{1} (1-u)^{\alpha}(1+u)^{\beta} \, P_k^{(\alpha,\beta)}(u) \, \Psi(u) du \ , \qquad (A.12)$$

$$h_k = \int_{-1}^{1} (1-u)^{\alpha}(1+u)^{\beta} \, [P_k^{(\alpha,\beta)}(u)]^2 \, du$$

$$= \frac{2^{\alpha+\beta+1}\,\Gamma(n+\alpha+1)\Gamma(n+\beta+1)}{(2n+\alpha+\beta+1)n!\Gamma(n+\alpha+\beta+1)} \quad ,$$

and $\quad \Psi(u) = \left(\frac{b}{1-u}\right)^{a} F\left(\frac{b}{1-u}\right) \quad .$ (A.13)

All the basic orthogonality properties for Jacobi polynomials may be found in Abramovitz and Stegun (1965).

Equation (A.11) may be inverted term by term, Roberts and Kaufman (1966) to obtain

$$f(t) = \frac{t^{a-1}}{\Gamma(a)} \sum_{k=o}^{\infty} \frac{c_k}{k!} \frac{\Gamma(k+\alpha+1)}{\Gamma(\alpha+1)} \phi_k\,(bt/2) \qquad (A.14)$$

where $\phi_k(x) = {}_2F_2\left[\begin{matrix}-k\,, & k+\alpha+\beta+1 \\ \alpha+1\,, & a\end{matrix}\,;\, x\right]$ is the generalized hyper-geometric function. Its accurate evaluation for high k is difficult as a power series.

These formulas are too complex for casual use and Piessens simplifies the equation by putting $\alpha = \beta = -\frac{1}{2}$, and truncating (A.14) after M + 1 terms, and (A.12) after N + 1 terms. We then have

$$f(t) = \frac{t^{a-1}}{\Gamma(a)} \sum_{k=o}^{M\prime} c_k\ \phi_k\,(bt/2) \qquad (A.15)$$

where $\quad \phi_k(x) = {}_2F_2\left[\begin{matrix}-k, k \\ \frac{1}{2}, a\end{matrix}\,;\, x\right]$ (A.16)

and $\quad c_k = \frac{2}{N} \sum_{m=o}^{N\prime\prime} \Psi(\cos\tfrac{\pi m}{N}) \cos\tfrac{\pi mk}{N} \quad .$ (A.17)

Equation (A.17) requires that $\Psi(1)$ must exist. That is, from (A.13), $\lim_{s\to\infty} s^{a}F(s)$ must exist. The functions in

sections 6.2 and 6.3 do satisfy this condition providing we choose $a = 1.5$ and 2 respectively. For convenience we also choose $M = N$.

Finally Piessens proposes an algorithm to evaluate the ϕ_k without a large loss of significance, (a common fault with other methods):

$$\phi_n + (A + Bx)\phi_{n-1} + (C+Dx)\phi_{n-2} + E\phi_{n-3} = 0$$

$$n = 3 , 4 \ldots$$

where $\phi_o = 1$, $\phi_1 = 1 - 2x/a$, $\phi_2 = 1 - 8x/a + 8x^2/a(a+1)$

and $A = \frac{1}{2}(2n-3)(n+a-2)/(n+a-1) - 2n$.

$$B = 4/(n+a-1)$$
$$D = (n-1)B/(n-2)$$
$$E = -D(n-a-2)/4$$
$$C = -1-A-E .$$

The only parameter remaining to be chosen is b . The expansion (A.11) is valid for all $s \in [b/2 , \infty)$, and thus we choose b small, but not so small that convergence of (A.11) is too slow.

A double precision test program was written to duplicate some of the results of Piessens method presented in his paper. The function $J_o(t)$ was evaluated by inverting $(s^2+1)^{-\frac{1}{2}}$ and very high accuracy achieved, actually better by a factor of 5-10 than Piessens results, carried out on an IBM 360/44.

Nordens method on the other hand produced poor results for this function, as did the B-K-L method. This is in contrast to their success and the failure of the Piessens method in inverting the functions of chapter six.

PROGRAM HALF-TIME

```
      DOUBLE PRECISION XO,TO,W(20,20),C(20),B,V1(2),U,V,PI,
     1SUM,F,F1,X,S(20),T,FLA,AL,SP,SA,SB,Y1,Y2,Y3,P,DITS
      DIMENSION JC(20)
      COMMON U,V,PI,AL,SP
      PI=3.1415926535897932D0
      XO=DEXP(-.6)
      B=DEXP(.2)
      SP=1.0D0
      DITS=9.456D0
      N=10
      N1=N+1
      DO 11 I=1,N
      S(I)=0.5D0*DFLOAT(I)
      DO 11 J=1,N
      W(I,J)=B**(-S(I)*DFLOAT(J))
   11 CONTINUE
      CALL GAMMA(S,C)
      DO 3 I=1,N
      C(I)=XO**S(I)/C(I)
      W(I,N1)=C(I)
    3 CONTINUE
      V1(I)=4.0D0
      CALL DGJR (W,20,20,N,N1,$2,JC,V1)
      DO 10 I=1,N
   10 C(I)=W(I,N1)
      DO 1 I=1.4
      PRINT 200,SP
  200 FORMAT (1H1,5X24HPARTITION COEFFICIENT,SP ,F6.3/)
      PRINT 205 , DITS
  205 FORMAT (1H ,5X20HDIFFUSION TIME SCALE,3X,
     1F7.3,2X7HMINUTES/)AL=.2D0/DFLOAT(I)
      Y1=1.0D0/AL
      PRINT 201, Y1
  201 FORMAT(1H ,5X17HVASCULARITY,ALPHA,8X2H1/,F3.0/)
      PRINT 203
  203 FORMAT (7X3HLOG,20X3HLOG)
      PRINT 202
  202 FORMAT (5X9HPERFUSION,8X17HTISSUE HALF-TIMES)
      PRINT 204
  204 FORMAT (22X8HHENNESSY,2X7HHALDANE/)
      U=SP*(1.0D0-AL**2)/AL**2
      T=15.0D0
      DO 1 J=1,21
      Y1=.25D0*(5.0D0-J)
      P=10.0D0**Y1
      V=DITS*P/AL**4
      IF (V.LT.1000.0D0) GO TO 41
      F1=1.0D0/(1.0D0+U)
      GO TO 40
   41 F1=V/(1.0D0+U)
   40 SA=0.0D0
      SB=0.0D0
      L=1
    6 TO=T/B
      SUM=0.0D0
      DO 80 K=1,N
```

```
      X=XO*B**(K-1)/TO
   80 SUM=SUM+C(K)*FLA(X)
      F=F1*SUM/T
      Y1=F-.5DO
      Y2=DABS(Y1)
      IF (Y2.LE..1D-5) GO TO 8
      IF (L.GE.30) GO TO 7
      IF(Y1.LT.0.0DO) GO TO 19
      SB=T
      GO TO 5
   19 SA=T
      IF(SB) 17,17,5
   17 T=2.0DO*T
      GO TO 6
    5 T=.5DO*(SA+SB)
      L=L+1
      GO TO 6
    7 T=0.0DO
      PRINT 30
   30 FORMAT (17HFAILS TO CONVERGE/)
    8 Y1=DLOG(P)/DLOG(10.0DO)
      Y2=DLOG(DITS*T/AL**2)/DLOG(10.0DO)
      Y3=DLOG(AL**2*(1.0DO+U)*DLOG(2.0DO)/P)/DLOG(10.0DO)
      PRINT 20, Y1,Y2,Y3
   20 FORMAT (1H ,F10.2,8X,2F10.5)
    1 CONTINUE
      GO TO 4
    2 PRINT 100, JC(1),v1(1)
  100 FORMAT (1H 17HOVERFLOW DETECTED,5XI5,D20.5)
    4 END



      FUNCTION FLA(X)
      DOUBLE PRECISION  U,V,PI,FLA,X,Y1,Y2,Y3,SA,
     1SQA,AL,SP,BI1,BI2,BI3,BK1,BK2,BK3,SQ ,Y4
      COMMON U,V,PI,AL,SP
      SA=2.0DO*SP/AL
      SQ=DSQRT(X)
      SQA=SQ*AL
      M=1
      N=1
      CALL DBES(M,N,SQA,BI1)
      CALL DBES(M,N,SQ,BI2)
      N=0
      CALL DBES(M,N,SQA,BI3)
      M=2
      N=1
      CALL DBES(M,N,SQ,BK1)
      CALL DBES(M,N,SQA,BK2)
      N=0
      CALL DBES(M,N,SQA,BK3)
      Y1=BI1*BK1-BI2*BK2
      Y2=BI3*BK1+BI2*BK3
```

```
      Y3=X-SA*SQ*Y1/Y2
      Y4=Y3/V
      IF (V.GE.1000.0D0) GO TO 2
      FLA=(1.0D0-DEXP(-Y3/V))/X**2
      RETURN
    2 FLA=Y3*(1.0D0-.5D0*Y4+Y4**2/6.0D0-Y4**3/
     124.0D0+Y4**4/120.0D0-Y4**5/720.0D0)/X**2
      RETURN
      END
```

APPENDIX B

BESSEL FUNCTION EVALUATION

The modified Bessel functions I_o , I_1 , K_o and K_1 are required to be evaluated in double precision. Unfortunately standard library software is only available in single precision, and so a special program was written.

There are a number of methods available. At first a standard series approach was used, with the switchover points of I_o , I_1 and K_o K_1 to the asymptotic series being empirically adjusted to give the highest overall accuracy.

Whilst it was possible to obtain 16 to 17 figure accuracy, there was a zone near $x = 8$ where only 7 to 8 figure accuracy could be expected, and so the method was abandoned.

The final choice made was based on accuracy and ease of programming, with little regard to execution time economics. The method used is described in Luke (1969). We write

$$I_o(x) = \sum_{n=o}^{18} a_n T_{2n}(x/8) \qquad x \leq 8$$

$$= \frac{e^x}{\sqrt{2\pi x}} \sum_{n=o}^{33} c_n T_n^*(8/x) \qquad x > 8$$

$$I_1(x) = \sum_{n=o}^{17} a'_n T_{2n+1}(x/8) \qquad x \leq 8$$

$$= \frac{e^x}{\sqrt{2\pi x}} \sum_{n=o}^{33} d'_n T_n^*(8/x) \qquad x > 8$$

$$K_o(x) = -(\gamma+\log x/2) I_o(x) + \sum_{n=o}^{18} b_n T_{2n}(x/8) \qquad x \leq 8$$

$$= \sqrt{\pi/2x}\, e^{-x} \sum_{n=o}^{20} d_n T_n^*(5/x) \qquad x > 5$$

$$K_1(x) = (\gamma+\log x/2)I_1+1/x - \sum_{n=o}^{17} c_n' T_{2n+1}(x/8) \qquad x \leq 8$$

$$= \sqrt{\frac{\pi}{2x}}\ e^{-x} \sum_{n=o}^{20} e_n' T_n^*(5/x) \qquad x > 5$$

where $T_n(x)$ and $T_n^*(x)$ are the Chebyshev polynomials and shifted polynomials of the first kind respectively. Luke provides the coefficients a_i , b_i , c_i , d_i , a_i' , c_i' . d_i' , e_i' to 20 decimal places, rounded from 25 places.

The Chebyshev polynomials were evaluated by Clenshaws (1955) algorithm.

Suppose

$f_N(x) = \sum_{n=o}^{N} a_n g_n(x)$, where a_n is given and g_n is a Chebyshev polynomial, set up an algorithm as follows :

$$b_{n+2} = 0$$

$$b_{n+1} = 0$$

$$b_n = -\alpha\, b_{n+1} - b_{n+2} + a_n \ , \quad n = N, N-1, \ldots 2, 1, 0.$$

Then

$$f_N(x) = \begin{cases} b_o - (2x^2 - 1)b_1 \\ x(b_o - b_1) \\ b_o - (2x - 1)b_1 \end{cases}$$

according as

$$g_n(x) = \begin{cases} T_{2n}(x) \\ T_{2n+1}(x) \\ T_n^*(x) \end{cases} \qquad \text{and } \alpha = \begin{cases} -2(2x^2-1) \\ -2(2x^2-1) \\ -2(2x-1) \end{cases}$$

Because of the high accuracy of the coefficients, this method is probably the most accurate available. The results of a test program showed that 17 figure accuracy could be expected for large x .

The Wronskian $W = I_o K_1 + I_1 K_o = \frac{1}{x}$ was calculated and printed out in the form $W - 1/x$ to give an indication of accuracy. It was found that at least 12 figure accuracy is available. The high 17 figure accuracy for $x > 5$ was due to K_o and K_1 being evaluated by the asymptotic formulae which are much more accurate. The reason for this is that about five figures of accuracy is lost in evaluating K_o (also K_1) for $x \lesssim 5$ by the formula

$$K_o = - (\gamma + \log x/2)\, I_o(x) + \Sigma\, b_n\, T_{2n}(x/8)$$

Here as x increases, $I_o(x)$ and $\Sigma\, b_n\, T_{2n}(x/8)$ increase monotonely and $K_o(x)$ decreases, with consequent loss of precision. Essentially, a high precision is required in calculations of this type.

APPENDIX C

The roots of Cosh $\sqrt{\theta}$

We recall that in chapter 2, it was stated that the roots of $\cosh \sqrt{\theta} = 0$, where

$$\lambda\theta = s + 2\mu\sqrt{s}\, I_1(\sqrt{s})/I_o(\sqrt{s})$$

are all real and negative. A proof by the writer is given here.

It is easily seen that $\cosh \sqrt{\theta} = 0$ has a set of simple pure imaginary roots of the form

$$\sqrt{\theta} = (2n + 1)\pi i/2 \ , \quad n = 0 \ , 1 \ , 2 \ \ldots$$

Thus

$$s + 2\mu \sqrt{s}\, I_1(\sqrt{s})/I_o(\sqrt{s}) = - (2n+1)^2\pi^2\lambda/4 \ ,$$
$$= -\gamma^2 \ , < 0 \ . \qquad (C.1)$$

Put $\sqrt{s} = z = x + iy$ and substitute into (C.1) to obtain

$$z^2 + 2\mu z \frac{d}{dz} \log I_o(z) = - \gamma^2 \ ,$$

where $I_o'(z) = I_1(z)$

Divide by z , put $z = x + iy$ and take the real part to obtain

$$x + \mu \frac{\partial}{\partial x} \log |I_o(z)|^2 = - \frac{\gamma^2}{x^2+y^2} \ ,$$

where we have used $\frac{\partial}{\partial x} = \frac{\partial z}{\partial x} \frac{d}{dz} = \frac{d}{dz}$.

Thus

$$x \left(\frac{x^2+y^2+\gamma^2}{x^2+y^2}\right) + \mu \frac{\partial}{\partial x} \log |I_o(z)|^2 = 0 \ . \qquad (C.2)$$

At this stage it cannot be asserted that the last term is > 0 .

However, from Abramovitz and Stegun (1965) we have

$$I_o(z) = \prod_{i=1}^{\infty} (z^2 + \alpha_i^2)/\alpha_i^2$$

where α_i are the real roots of $J_o(z) = 0$.

Thus $$\log |I_o(z)|^2 = \sum_{i=1}^{\infty} \log(|z^2 + \alpha_i^2|^2/\alpha_i^2)$$

and it is easily shown that

$$\frac{\partial}{\partial x} \log |I_o(z)|^2 = \sum_{i=1}^{\infty} \frac{4x(x^2+y^2+\alpha_i^2)}{|z^2+\alpha_i^2|^2}$$

Substituting this result into (C.2), we have

$$x \left\{ (x^2+y^2+\gamma^2)/(x^2+y^2) + 4\mu \sum_{i=1}^{\infty} \frac{(x^2+y^2+\alpha_i^2)}{|z^2+\alpha_i^2|^2} \right\} = 0$$

Thus it follows that x must be zero

hence $\sqrt{s} = z = iy$

Thus $s = -y^2$ and the roots of $\cosh \sqrt{\theta} = 0$ are

s = real negative numbers satisfying

$$y^2 + 2\mu y \, J_i(y)/J_o(y) = \gamma^2 \quad .$$

APPENDIX D

PUBLICATIONS EXTRACTED FROM THESIS

The following monographs were extracted from the thesis.

Chapter 2: Inert Gas Diffusion in Heterogeneous Tissue I Without Perfusion.
Bull.Math.Biophysics, 33, 235-248, 1971

Chapter 3: Inert Gas Diffusion in Heterogeneous Tissue II With Perfusion.
Bull.Math.Biophysics 33, 249-257, 1971

Chapter 4: The Equivalent Bulk Diffusion Model of the Pneumatic Decompression Computer.
Med.Biol.Engg. 11, No 3, 1973.

In addition:

Chapters 5 and 6: The Interaction of Perfusion and Diffusion in Homogeneous Tissue.
To be submitted to Bull.Math.Biophysics.

ACKNOWLEDGEMENTS

The work was carried out whilst a lecturer in the Department of Applied Mathematics, University of Cape Town, and I thank the University for their support of the interdisciplinary field of Mathematical Biophysics.

I also thank the following:

G.B. Brundrit, Ph.D, and Prof. J.J.W. van Zyl, M.D. who willingly agreed to act as supervisors.

Dr. B.A. Hills for his very helpful advice and encouragement.

The late Prof. N. Rashevsky, for his personal interest and encouragement, especially during his visit to Cape Town, 1971.

My wife Debbie for her sterling support over the years, and checking the proofs.

Mrs. B. Tindale for her excellent layout and typing.

BIBLIOGRAPHY

Abramovitz, M. and Stegun, I.A. (eds), 1965. *Handbook of Mathematical Functions.* New York: Dover.

Atkinson, M.P. and Lang, S.R. 1972 . *A Comparison of some Inverse Laplace Transform Techniques for use in Circuit Design.* Comp. Journal 15, 138-139.

Bell, G.H., Davidson, J.N. and Scarborough, H. 1961. *Textbook of Physiology and Biochemistry.* London: Livingstone.

Bellman, R., Jacquez, J.A. and Kalaba, R. 1960. *Some Mathematical Aspects of Chemotherapy: I. One-Organ Models.* Bull. Math Biophysics 22, 181-198.

Bellman, R., Kalaba, R., and Lockett, J-A. 1966. *Numerical Inversion of the Laplace Transform.* New York: American Elsevier.

Blum, J.J. 1960. *Concentration Profiles in and around Capillaries.* Am. J. Physiol. 198, 991-998.

Boycott, A.E., Damant, G.C.C., and Haldane, J.S. 1908. *The Prevention of Compressed Air Illness.* J. Hyg. 8, 342-443.

Carslaw, H.S. and Jaeger, J.C. 1959. *Conduction of Heat in Solids.* London: Oxford.

Churchill, R.V. 1958. *Operational Mathematics.* New York: McGraw-Hill.

Clenshaw, C.W. 1955. *A Note on the Summation of Chebyshev Series.* MTAC 9, 118-120.

Crank, J. 1956. *Mathematics of Diffusion.* London: Oxford.

Dick, D.A.T. 1959. *The Rate of Diffusion of Water in the Protoplasm of Living Cells.* Exp. Cell. Res. 17, 5-12.

Dubner, H. and Abate, J. 1968. *Numerical Inversion of the Laplace Transform by Relating them to the Finite Fourier Cosine Transform.* J.A.C.M. 15, 115-123.

Eaton, W.J. 1970. *Investigation into the Decompression Tables; a Practical Approach to the Evaluation of Safe Decompression Procedures.* Rev. Subaquat. Physiol. 2, 8-15.

Erdelyi, A. 1943. *Inversion Formulae for the Laplace Transform.* Phil. Mag. 34, 533-536.

Fenichel, I.R. and Horowitz, S.B. 1963. *The Transport of Non-Electrolytes in Muscle as a Diffusional Process in Cytoplasm.* Acta physiol. Scand. 60 Suppl. 221 , 1-63.

Gonzalez-Fernandez, J.M. and Atta, S.E. 1972. *Concentration of Oxygen around Capillaries in Polygonal Regions of Supply.* Math. Biosci. 13, 55-69.

Guyton, A.C. 1969. *Textbook of Medical Physiology.* Philadelphia: Saunders.

Haldane, J.S. See under Boycott, Damant and Haldane (1908).

Hansson Mild, K. 1972. *Diffusion Exchange between a Membrane-Bounded Sphere and its Surrounding.* Bull. Math. Biophysics 34, 93-102.

Harris, E.J. and Burn, G.P. 1949. *The Transfer of Sodium and Potassium Ions between Muscle and the Surrounding Medium.* Trans. Farad. Soc. 45, 508-528.

Hempleman, H.V. 1967. *Decompression Procedures for Deep, Open Sea Operations.* In *'Proceedings of the Third Symposium of Underwater Physiology'*. Ed. Lambertsen, C.J., Baltimore: Williams and Wilkins.

Hempleman, H.V. 1969. *British Decompression Theory.* In *'The Physiology and Medicine of Diving'*, Bennett, P.B. and Elliott, D.H. (eds.). London: Baillére, Tindall and Cassell.

Hennessy, T.R. 1971a. *Inert Gas Diffusion in Heterogeneous Tissue I. Without Perfusion.* Bull. Math. Biophysics 33, 235-248.

Hennessy, T.R. 1971 b. *Inert Gas Diffusion in Heterogeneous Tissue II. With Perfusion.* Bull. Math. Biophysics 33, 249-257.

Hennessy, T.R. 1973. *The Equivalent Bulk-Diffusion Model of the Pneumatic Decompression Computer.* Med. and Biol. Engng. 11, No. 3.

Hills, B.A. 1966. *A Thermodynamic and Kinetic Approach to Decompression Sickness.* Libraries Board of South Australia, Adelaide.

Hills, B.A. 1967a. *A Pneumatic Analogue for Predicting the Occurrence of Decompression Sickness.* Med. and Biol. Engng. 5, 421-432.

Hills, B.A. 1967b. *Diffusion versus Blood Perfusion in Limiting the Rate of Uptake of Inert Non-Polar Gases by Skeletal Rabbit Muscle.* Clin. Sci. 33, 67-87.

Hills, B.A. 1968. *Linear Bulk Diffusion in Heterogeneous Tissue.* Bull. Math. Biophysics 30, 47-59.

Hills, B.A. 1969a. *Radial Bulk Diffusion into Heterogeneous Tissue.* Bull. Math. Biophysics 31, 25-34.

Hills, B.A. 1969b. *Thermodynamic Decompression.* In '*The Physiology and Medicine of Diving*'. Bennett, P.B. and Elliott, D.H. (eds.). London: Baillére, Tindall and Cassell.

Hills, B.A. 1969c. *The Time Course for the Uptake of Inert Gases by the Tissue Type responsible for Marginal Symptoms of Decompression Sickness.* Rev. Subaquat. Physiol. 1, 255-261.

Hills, B.A. 1970a. *Respiration of Tissue as a Medium of Heterogeneous Permeability.* Bull. Math. Biophysics 32, 219-235.

Hills, B.A. 1970b. *An Assessment of the Expression* $C = \mathring{Q}[1 - exp(- PS/\mathring{Q})]$ *for Estimating Capillary Permeabilities.* Phys. Med. Biol. 15, 705-713.

Hills, B.A. 1970c. *Vital Issues in Computing Decompression Schedules from Fundamentals II. Diffusion Versus Blood Perfusion in Controlling Blood-Tissue Exchange.* Int. J. Biometeor 14, 323-342.

Kety, S.S. 1951. *The Theory and Applications of the Exchange of Inert Gas at the Lungs and Tissues.* Pharm. Rev. 3, 1-41.

Kidd, D.J. and Stubbs, R.A. 1969. *The Use of the Pneumatic Analogue Computer for Divers.* In '*The Physiology and Medicine of Diving*', p 386-413. Ed. Bennett, P.B. and Elliott, D.H. London: Bailliére, Tindall and Cassell.

Kidd, D.J., Stubbs, R.A. and Weaver, R.S. 1970. *Comparative Approaches to Prophylactic Decompression.* In '*Proceedings of the Fourth Symposium of Underwater Physiology*'. Ed. Lambertsen, New York: Academic.

Krogh, A. 1919a. *The Rate of Diffusion of Gases through Animal Tissues, with some remarks on the Coefficient of Invasion.* J. Physiol. 52, 391-408.

Krogh, A. 1919b. *The Number and Distribution of Capillaries in Muscles with Calculations of the Oxygen Pressure Head Necessary for Supplying Tissue.* J. Physiol. 52, 409-415.

Krogh, A. 1919c. *The Supply of Oxygen to the Tissues and the Regulation of the Capillary Circulation.* J. Physiol. 52, 457-474.

Krogh, A. 1936. *The Anatomy and Physiology of Capillaries.* Yale University Press, New Haven.

Krylov, V.I. and Skoblya, N.S. 1969. *Handbook of Numerical Inversion of Laplace Transforms.* Jerusalem: Israeli program for Scientific Translations.

Lanczos, C. 1956. *Applied Analysis.* Englewood Cliffs, New Jersey: Prentice Hall.

Longman, I.M. 1972. *Numerical Laplace Transform Inversion of a Function arising in Visco Elasticity.* J. Comput. Physics 10, 224-231.

Luke, Y. 1969. *The Special Functions and their Approximations. Vols. I and II.* New York: Academic.

Miller, M.K. and Guy, W.T., Jr. 1966. *Numerical Inversion of the Laplace Transform by use of Jacobi Polynomials.* SIAM J. Numer. Anal. 3, 624-635.

Morales, M.F., Smith, R.E. 1944. *On the Theory of Blood-Tissue Exchanges: III Circulation and Inert-Gas Exchanges at the Lung with Special Reference to Saturation.* Bull. Math. Biophysics 6, 141-152.

Morales, M.F., Smith, R.E. 1945a. *A Note on the Physiological Arrangement of Tissues.* Bull. Math. Biophysics 7, 47-51.

Morales, M.F., Smith, R.E. 1945b. *The Physiological Factors which Govern Inert Gas Exchange.* Bull. Math. Biophysics 7, 99-106.

Morales, M.F., Smith, R.E. 1948. *On the Theory of Blood-Tissue Exchange of Inert gases: VI. Validity of Approximate Uptake Expressions.* Bull. Math. Biophysics 10, 191-200.

Norden, H. 1961. *Numerical Inversion of the Laplace Transform.* Acta Acad. Aboensis Math. et Phys. 22, No. 8, 1-31.

Norden, H. 1962. *Transient Heat Conduction in a Semi-Infinite Cylindrical Wire enclosed by a Homogeneous Solid.* Acta Acad. Aboensis Math et Phys. 22, No. 9, 1-71.

Norden, H. and Seppä, I. 1964. *A Problem in Heat Conduction in a Wire enclosed by a Cylindrical Material Solved by Numerical Inversion of the Laplace Transform.* Nordisk. Tidskrift. fur Informations behandling 4, 224-242.

Opatowski, I. and Schmidt, G.W. 1952. *Determination of Diffusion and Permeability Coefficients in Muscle.* Bull. Math. Biophysics 14, 45-65.

Piessens, R. 1969a. *New Quadrature Formulas for the Numerical Inversion of the Laplace Transform.* B.I.T. 9, 351-361.

Piessens, R. 1969b. *Numerical Inversion of the Laplace Transform.* IEEE Trans. Automat. Control. AC-14, 299-301.

Piessens, R. 1972. *A New Method for the Inversion of the Laplace Transform.* J. Inst. Maths. Applics. 10, 185-192.

Roberts, G.E. and Kaufman, H. 1966. *Table of Laplace Transforms.* Philadelphia: Saunders.

Roughton, F.J.W. 1952. *Diffusion and Chemical Reaction Velocity in Cylindrical and Spherical Systems of Physiological Interest.* Proc. Roy. Soc. B 140, 203-221.

Salzer, H.E. 1958. *Tables for the Numerical Calculation of Inverse Laplace Transforms.* J. Math. Phys. 37, 89-109.

Sangren, W.C., Sheppard, C.W. 1953. *A Mathematical Derivation of the Exchange of a Labelled Substance between a Liquid flowing in a Vessel and an External Compartment.* Bull. Math. Biophysics 15, 387-394.

Schmidt, G.W. 1952. *A Mathematical Theory of Capillary Exchange as a Function of Tissue Structure.* Bull. Math. Biophysics 14, 229-263.

Schmidt, G.W. 1953. *The Time Course of Capillary Exchange.* Bull. Math. Biophysics 15, 477-488.

Shirtliffe, C.J. and Stephenson, D.G. 1961. *A Computer Orientated Adaptation of Salzer's Method for Inverting Laplace Transforms.* J. Math. Phys. 40, 135-141.

Smith, R.E., Morales, M.F. 1944a. *On the Theory of Blood Tissue Exchanges. I Fundamental Equations.* Bull. Math. Biophysics 6, 125-132.

Smith, R.E., Morales, M.F. 1944b. *On the Theory of Blood Tissue Exchanges. II Applications.* Bull. Math. Biophysics, 6, 133-139.

Stehfest, H. 1970. *Algorithm 368.* CACM 13, No. 1.

Stubbs, R.A. and Kidd, D.J. 1965. *A Pneumatic Analogue Decompression Computer.* Canadian Forces Medical Service, Institute of Aviation Medicine Report 65-RD-1.

Stubbs, R.A.,and Weaver, R.S. 1968. *The Transient Response of an M-Loop Series Filter System with special application to the Decompression Problem in Man. Linear Model.* Defense Research Establishment Toronto. DRET Research Paper No. 620.

Taylor, G.I. 1953. *Dispersion of Soluble Matter in Solvent Flowing slowly through a Tube.* Proc. Roy. Soc. A 219 186-203.

Teorell, T. 1937. *Kinetics of Distribution of Substances Administered to the Body. I. The Extra-Vascular Modes of Administration.* Arch. internat. de Pharmacodyn. et de thérap. 57, 205-224.

Thews, G. 1953. *Über Die Mathematische Behandling Physiologischer Diffusion Prozesse in Zylinderförmigen Objekten.* Acta Bio theoretica 10, 105-137.

Van Liew, H.D. 1962. *Semi-Logarithmic Plots of Data which reflects a Continuum of Exponential Processes.* Science 138, 682-683.

Von Schrotter, H. 1906. *Der Sauerstoff in der Prophylaxe und Therapie der Luft druckerkrankungen.* In Michaelis M., Handbuch der Sauerstofftherapie, Berlin: Hirschwald. *Cited by Kety (1951).*

Weaver, R.S. and Stubbs, R.A. 1968. *The Transient Response of an M-Loop Series Filter System with Special Application to the Decompression Problem in Man. Non Linear Model.* DRET Research Paper No. 674.

Weaver, R.S., Kuehn, L.A. and Stubbs, R.A. 1968. *Decompression Calculations: Analogue and Digital Methods.* DRET Report No. 703.

Zakian, V. 1969. *Numerical Inversion of the La place Transform.* Electronics Letters 5, 120-121.

Zuntz, N. 1897. *Zur Pathogenese und Therapie der durch rasche Luftdruckanderungen erzeugten Krankheiten.* Fortschr. d. Med. 15, 632-639. *Cited by Kety (1951).*

TABLE OF NOTATION AND SYMBOLS

The following is a representative (but not exhaustive) list of symbols and notation that appear in the text.

a	cell radius, chap. 2,3 ; capillary radius, chap.5 (cm)
b	outer radius extracellular annulus, chap.2, 3 (cm) extracapillary annulus, chap.5.
D	diffusion coefficient of inert gas (cm^2 sec^{-1})
D_c	diffusion coefficient of gas in cellular phase.
D_e	diffusion coefficient of gas in extracellular phase.
f	volume fraction of extracellular fluid.
k	exponential time constant (min^{-1}).
ℓ	length of tissue slice, chap.2 (cm). length of capillary, chap. 5.
$M(t)$	mass uptake of inert gas (gm)
M_o	initial mass of gas in tissue zone.
M_∞	final mass of gas in tissue zone.
P	Blood perfusion (ml blood/ml tissue/min), chap.5.
P_o	initial gas tension in tissue, (atmospheres).
P_1	ambient gas tension of hyperbaric environment.
$p(t)$	average gas tension in tissue zone.
p_a	arterial gas tension.
$p_b(z,t)$	gas tension in capillary, chap. 5.
$p_c(r,t)$	gas tension in cellular phase.
$p_e(t)$	gas tension in extracellular phase.
p_v	venous gas tension.
$\mathring{Q}$	blood perfusion.
$\mathring{Q}_e$	extracellular blood perfusion (includes possible lymph drainage).
r	radial coordinate (cm).
s	Laplace Transform parameter

S_b gas solubility in blood, (gm gas/ml blood/atmosphere at $37^{\circ}C$).

S_c gas solubility in cellular phase.

S_e gas solubility in extracellular phase.

S_p partition coefficient S_c/S_e chap. 2,3 ; S_c/S_b, chap,5.

t time variable (seconds or dimensionless).

T, T_H tissue half-time (min. or dimensionless)

T_c cellular diffusion time-scale (min).

T_I interstitial diffusion time-scale.

T_P perfusion time-scale.

V blood velocity in capillary, cm sec^{-1} .

z axial coordinate (cm)

α vascularity; a/b, chap. 5.

λ diffusion time-scale in cells/extracellular phase, $(a^2/D_c)/(\ell^2/D_e)$, chap. 2.
diffusion time-scale in cells/perfusion time scale, $(a^2/D_c)(\ell/\dot{Q}_e)$, chap. 3
$(b^2/D_c)/(\ell/V)$, chap. 5.

θ see equation 2.14.

μ gas capacity of cells/gas capacity of extracellular phase, $a^2S_c/((b^2-a^2)S_e)$, chap. 2, 3, 5.